LRP8 is a Receptor for Yellow Fever Virus

Miao Mei[1*], Yang Yang[2*], Zihan Zhang[3*], Yue Yin[2], Jiali Tan[1], Chao Jiang[1], Yu Gao[1], Zhaoyang Wang[4], Donghong Wang[5], Yajing Li[1], Yingyi Cong[1], Zhiyuan Zhang[6], Yousong Peng[6], Wenjie Tan[7], Jiandong Li[7], Li Li[8], Hanxue Wang[9], Ren Lang[9], Qiang He[9], Zihou Deng[8], Xiaojie Huang[10], Bin Luo[11], Cao Shan[3], Yonghong Zhang[10], Lin Mei[11], Gong Cheng[4], Xu Tan[1#]

1. Chinese Institute for Immunology, Chinese Institutes for Medical Research, Beijing You'an Hospital, Capital Medical University, Beijing, China
2. Shenzhen Key Laboratory of Pathogen and Immunity, National Clinical Research Center for infectious disease, State Key Discipline of Infectious Disease, Shenzhen Third People's Hospital, Second Hospital Affiliated to Southern University of Science and Technology, Shenzhen, China
3. State Key Laboratory of Virology and Biosafety, Wuhan Institute of Virology, Chinese Academy of Sciences, Wuhan 430071, China; University of the Chinese Academy of Sciences, Beijing 100039, China; Center for Biosafety Mega-Science, Wuhan Institute of Virology, Chinese Academy of Sciences, Wuhan 430071, China; Hubei Jiangxia Laboratory, Wuhan 430200, China
4. Tsinghua-Peking Center for Life Sciences, School of Medicine, Tsinghua University, Beijing; Institute of Infectious Diseases, Shenzhen Bay Laboratory, Shenzhen, China
5. School of Medicine, Tsinghua University, Beijing
6. Bioinformatics Center of College of Biology, Hunan Provincial Key Laboratory of Medical Virology, Hunan University, Changsha, China.
7. NHC Key Laboratory of Biosafety, National Institute for Viral Disease Control and Prevention, Chinese Center for Disease Control and Prevention, Beijing, 102206, China.
8. Chinese Institute for Cancer Research, Chinese Institutes for Medical Research, Capital Medical University, Beijing, China
9. Department of Hepatobiliary and Pancreatic Surgery, Beijing Chao-Yang Hospital, Capital Medical University, Beijing, China
10. Beijing You'an Hospital, Capital Medical University, Beijing, China
11. Chinese Institutes for Medical Research, Capital Medical University Beijing, China

*: These authors contributed equally to this work

#: Correspondence should be addressed to: Xu Tan (xtan@cimrbj.ac.cn)

Abstract

Yellow fever virus (YFV), an arbovirus causing substantial human morbidity and mortality, was the first human virus discovered over a century ago. The live-attenuated 17D vaccine is among the most successful vaccines in medicine. Despite the importance of YFV, its receptor has remained unknown. Here, we performed a barcoded, genome-wide human ORF library screen and identified LRP8 (also named APOER2) as a receptor for YFV. We show that LRP8 expression specifically boosts YFV infection in cell lines by promoting entry. AAV-mediated expression of human LRP8 in mouse liver aggravates infection and pathology. LRP8 knockdown abolishes YFV infection in brain cells, primary human hepatocytes, and notably in mosquitoes. Biochemically, LRP8 directly interacts with YFV particles via the viral envelope protein. This function of LRP8 is conserved across species, particularly in mosquitoes and primates. A soluble LRP8 decoy protein can block YFV infection in vitro and in mice, providing a potential therapeutic or prophylactic strategy. Our findings provide groundwork for understanding YFV entry, tropism, and pathogenesis, and may enable development of novel therapeutics to treat YFV infection.

Introduction

Yellow fever virus (YFV), the first human virus ever discovered, is among the deadliest human pathogens and has shaped human history[1-3]. Owing to the landmark discovery in 1900[4] that mosquitoes transmit YFV and subsequent public-health efforts—particularly development and wide application of the 17D vaccine—Yellow fever (YF) is no longer considered epidemic in most countries today[5]. However, the sylvatic transmission cycle of YFV, namely transmission between non-human primates via forest mosquitoes, makes elimination highly improbable. YF remains a significant public-health concern in tropical regions of South America and Africa, with an estimated 84,000–170,000 severe cases and 29,000–60,000 deaths per year[6]. Recent outbreaks occurred in Brazil, the Democratic Republic of the Congo, Angola, Uganda, and Nigeria, with spillover cases in Asia [7]. YFV infection causes hemorrhagic fever characterized by hepatitis and jaundice. YFV infects the liver and can induce disseminated intravascular coagulation, producing hemorrhagic manifestations[8]. In late stages, the central nervous system may be affected together with multiple organ failure preceding death[8].

The attenuated 17D vaccine, developed in the 1930s, has been administered to over 500 million people, greatly reducing the burden of YFV for decades. However, vaccine production constraints during emergent outbreaks hinder

rapid, comprehensive immunization[7,9]. In addition, rare serious adverse events such as Yellow Fever Vaccine-Associated Neurotropic Disease (YEL-AND) and Yellow Fever Vaccine-Associated Viscerotropic Disease (YEL-AVD) suggest directions for improvement in next-generation vaccines[10,11]. The 17D vaccine was obtained by serial passage of the Asibi strain in mouse brain and chicken embryos (>176 passages), resulting in reduced neuro- and viscerotropism. Sequencing pinpointed 20 amino-acid differences and four additional nucleotide differences between 17D and Asibi that underlie reduced virulence[12]. Among the 20 amino-acid changes, eight reside in the envelope (E) protein, which determines tropism by engaging cellular receptors and mediating entry.[12-16].

A better understanding of the YFV life cycle would clarify tropism, pathogenesis, and the mechanism of 17D attenuation. Currently, the identity of the specific cellular receptor for YF remains unknown, hampering a molecular understanding of entry and virulence[17]. Here, we describe a genome-wide gene-overexpression screen that identifies LRP8 (also named APOER2) as a receptor for YFV. We show that LRP8 is expressed in both liver and brain, illuminating the tissue tropism of YF. Our results also highlight the effectiveness of overexpression screening in identifying viral receptors that have resisted gene-downregulation approaches such as CRISPR-Cas9 and RNAi.

Genome-wide overexpression screen to identify LRP8 as a potential YFV receptor

To uncover the long-sought YFV receptor, we applied a barcoded ORFeome library covering more than 15,000 human genes in a lentivector system driven by a CMV promoter to facilitate stable expression in mammalian cells[18,19]. We performed the screen in HEK293T cells, which have intrinsically low susceptibility to YFV. Cells were transduced with the ORFeome library at low MOI (0.1) to ensure single-ORF expression per cell. After puromycin selection, cells were infected with a recombinant YFV reporter (GFP) virus (**Fig.1a**)[20]. GFP expression enabled flow-cytometric sorting to enrich infected cells. GFP-positive and GFP-negative populations were separately processed for genomic DNA extraction, followed by PCR amplification of the barcode region adjacent to the ORF C terminus. Deep sequencing quantified the relative abundance of each ORF in the two populations. The screen was performed twice, each in triplicate. Low-density lipoprotein receptor-related protein 8 (LRP8) consistently ranked among the top candidates enriched in GFP-positive cells (**Fig.1b and Supplementary Data Set**). LRP8 (ApoER2) belongs to the low-density lipoprotein receptor (LDLR) family [21]. It is known to

124 be expressed in the brain and plays crucial roles in neuronal development and
125 synaptic plasticity [22,23]. Previously, LRP8 together with VLDLR, another LDLR
126 family member, was identified as an entry receptor for certain alphaviruses
127 including Semliki Forest virus, eastern equine encephalitis virus, and Sindbis
128 virus[24]. However, to the best of our knowledge, no study implicated LRP8 in
129 flavivirus infection.
130
131 Overexpression of LRP8 dramatically enhanced infection by both 17D
132 pseudovirus, but not Zika pseudovirus, as shown by image quantification (**Fig.**
133 **1c and 1d**). Plaque assays showed that LRP8 significantly boosted infection
134 of YFV-17D live virus (**Fig. 1e**). Moreover, three major LRP8 isoforms showed
135 similar activity in promoting YF infection (**Extended Fig. 1a-1c**). In contrast,
136 overexpression of TIM1, a phosphoserine-binding protein, facilitated Zika
137 virus infection[25] and had much weaker effect on YFV infection (**Fig. 1c and 1d,**
138 **Extended Fig. 1e and 1f**). LDLR, the prototypic member of the LDLR family,
139 showed little effect on YFV infection in our ORFeome screen and validation
140 experiments (**Fig. 1b, 1c and 1d**). Because the ligand-binding domain (LBD)
141 of LRP8 mediates engagement of endogenous ligand Reelin and alphavirus
142 envelopes[12,26], we generated two LRP8 constructs: an LBD deletion (ΔLBD)
143 and an EGF-domain deletion (ΔEGF) control. Ectopic expression of
144 LRP8-ΔLBD lost the ability to promote YFV infection, whereas LRP8-ΔEGF
145 retained activity (**Extended Fig. 1a, 1b and 1d**), supporting a requirement for
146 the LBD. We also expressed LRP8 in K562 cells, a line with very low levels of
147 endogenous LRP8[24] and showed that it also promoted YFV-17D infection
148 (**Extended Fig. 2**). Beyond the 17D vaccine strain, we tested BJ01, a clinical
149 isolate of the Angola genotype derived from a rare spillover case in China[27].
150 YFV-BJ01 showed enhanced infection and replication dynamics as 17D in
151 LRP8-overexpressing cells (**Fig. 1e, 1f and 1g, Extended Fig 3a**). BJ01
152 pseudovirus infection was likewise enhanced by LRP8 (**Extended Fig. 3b**).
153 Pseudotyped particles bearing E proteins from Dengue virus, Japanese
154 encephalitis virus, West Nile virus, Sepik, or Wesselsbron viruses, the latter
155 two the closest to YFV based on genome analysis[28], did not exhibit increased
156 infection in LRP8-overexpressing cells (**Fig. 1h**). Overall, LRP8 promotes YFV
157 entry in a rather specific fashion among the viruses tested.
158
159 We also generated U87-MG *LRP8* knockout (KO) cells, a glioma-origin cell
160 line. The KO was validated by FACS analysis and Western blots (**Extended**
161 **Fig. 4a and Fig. 2a**) The *LRP8*-KO cells showed profound decreases in
162 infection by YFV 17D (**Fig. 2a, 2b and 2c**) and the clinical strains BJ01 and
163 Asibi (**Fig. 2d and 2e**). Importantly, this decrease was reversed by ectopic
164 expression of sgRNA-resistant LRP8 constructs with synonymous mutations
165 in sgRNA sites, ruling out CRISPR off-target effects (**Fig. 2f, 2g and 2h,**

166 **Extended Fig. 4c, 4d**). Consistently, knockout of LRP8 had no effect on Zika
167 virus infection (**Fig. 2a, 2b and 2c**). Moreover, an antibody targeting the
168 extracellular domain of LRP8 (sc-293472) blocked YFV but not Zika virus,
169 further supporting a cell-surface receptor role (**Fig. 2i**). This antibody did not
170 block YFV infection of the LRP-KO cells, demonstrating its specificity
171 (**Extended Fig. 4f**).
172
173 **LRP8 promotes the entry of YFV**
174
175 We next examined whether LRP8 affects the entry step using 17D. Viral
176 binding to cells was measured after 90 min at 4 °C, while internalization was
177 measured after 2 h at 37 °C. Overexpression of LRP8 significantly boosted
178 binding and subsequent internalization (**Fig. 3a**). Accordingly, LRP8 knockout
179 in U87-MG cells reduced YFV binding and internalization (**Fig. 3b and 3c**). An
180 E-targeting antibody similarly inhibited binding, serving a positive control (**Fig.**
181 **3b**). An imaging approach further showed that LRP8 expression promoted
182 binding and internalization of YFV virus-like particles (VLPs). Alexa Fluor
183 647-labeled YF17D VLPs were incubated with cells at 37 °C for 30 min,
184 washed extensively, and membranes were marked with FITC-WGA.
185 Compared to luciferase or LRP8-ΔLBD, LRP8 significantly increased the
186 number of VLPs at the membrane and in the cytoplasm (**Fig. 3d and 3e**), the
187 effect exceeded that of TIM1. In contrast, VLPs bearing Zika prM/E were not
188 significantly affected by LRP8 (**Fig. 3e and 3f**). Again, the LBD was required:
189 LRP8-ΔLBD and LDLR did not promote YFV entry (**Fig. 3d and 3e**).
190
191 **LRP8 interacts with the envelope protein of YFV**
192
193 We next tested whether LRP8 interacts with the YFV envelope protein, a
194 prerequisite for a bona fide receptor. We purified Fc-tagged LRP8-LBD
195 (LBD-Fc) and performed pulldown assays. YFV envelope protein was
196 specifically pulled down with LRP8 LBD-Fc but not LDLR LBD-Fc (**Fig. 3g**).
197 Biolayer interferometry (BLI) further measured the interaction. LRP8-LBD
198 immobilized on the sensor bound purified YF17D particles with fast, strong
199 kinetics, whereas LDLR-LBD did not (**Extended Fig. 5**). Conversely,
200 immobilized YFV particles bound soluble LRP8-LBD, allowing estimation of an
201 apparent affinity (Kd = 0.46 ± 0.13μM) (**Fig. 3h**). YF17D VLPs containing only
202 E and M proteins also bound LRP8-LBD with similar affinity (Kd = 0.30 ±
203 0.12μM) (**Fig. 3i**), together with the pull-down experiment, supporting a direct
204 E–LRP8 interaction,
205
206 **Profiling of potential receptor usages by YF17D and clinical YFV strains**
207

It has been demonstrated that VLDLR, another LDLR family protein highly homologous to LRP8, can serve as a receptor for alphaviruses. We therefore tested whether this applies to YFV. While LRP8 strongly promoted 17D, BJ01 and Asibi strains, VLDLR promoted infection by YF17D to a level similar to LRP8 but showed a weaker effect on YFV-BJ01 or Asibi compared with LRP8 (**Fig. 4a, 4b and 4c**). Screening other LDLR family members revealed that, in addition to LRP8 and VLDLR, only LRP4 promoted YF17D infection when overexpressed (**Fig. 4a and Extended Fig. 6**). Similar to VLDLR, LRP4 exhibited a weaker effect on BJ01 (**Fig. 4b**). For LRP1, full-length expression was not observed, likely due to its large size (>500 kDa), precluding conclusions (**Extended Fig. 6**). Interestingly, mouse LRP8 and mouse VLDLR, which promoted YF17D as strongly as human LRP8, supported Asibi pseudovirus and BJ01 only weakly if at all (**Fig.4a and 4b**). Because YF17D was passaged in mouse brain before chick embryos, adaptation to mouse LRP8 likely occurred during passage.

We also tested a panel of LRP8 homologs from different species by overexpression (**Fig. 4d, 4e and Extended Fig. 7 and 8**). Most homologs facilitated YFV infection, indicating strong conservation from mammals to mosquitoes and C. elegans. In contrast, BJ01 usage of LRP8 homologs was more restricted, consistent with the shared non-conserved residues that distinguish Asibi from YF17D (**Extended Fig. 9**).

LRP8 is expressed in human liver and mediates YFV infection in primary human hepatocytes and in a mouse model

LRP8 is well known to be highly expressed in brain, but its expression in human liver is less well characterized. Because liver is a key target organ of YFV, we assessed hepatic expression of LRP8 and homologs. Immunohistochemistry with two different LRP8 antibodies of human liver samples, showed clear LRP8 expression at levels comparable to brain (**Fig. 5a and Extended Fig. 10**). This was corroborated by Western blots and single cell sequencing data of human liver samples (**Fig. 5b and 5c)**. In contrast, LRP4 and VLDLR were low (**Fig. 5b and 5c)**.

Given LRP8 expression in the liver, we tested LRP8 knockdown in primary human hepatocytes using siRNAs. Two siRNAs significantly reduced infection of PHHs by YFV-17D and YFV-BJ01 relative to controls as measured by both cellular viral RNA levels and viral titers of the media, supporting a key role for LRP8 in human liver (**Fig. 5d-5i**). Accordingly, LRP8 decoy protein also blocked YFV infection of PHHs (**Extended Fig. 11a**).

To test human LRP8 in vivo, we used Adeno-associated virus (AAV) to overexpress LRP8 in the liver of AG129 mice, which are deficient in the interferon signaling pathway and thus useful for modeling YFV-associated viscerotropic disease[8]. The overexpression levels were confirmed by Western blots of the mouse livers (**Extended Fig. 11b**). Compared with LDLR overexpression (which does not promote YFV entry), LRP8 significantly aggravated pathology after BJ01 infection (**Fig. 5j**). Survival of mice with liver-specific LRP8 expression was significantly worse than with LDLR, correlating with higher viral titers, elevated MCP-1, and increased ALT/AST/bilirubin (**Fig. 5k-5p**). Survival in the LDLR group was similar to empty-AAV controls, further supporting LRP8-mediated enhancement in vivo.

LRP8 mediates YFV infection in mosquitoes

Because mosquitoes have a single LRP8/VLDLR-like gene (**Extended Fig. 7**), we used in vivo gene knockdown via injection of synthesized double-stranded RNA (dsRNA) targeting Aedes aegypti VLDLR in the thorax. Four dsRNAs effectively knocked down VLDLR, and correspondingly blocked infection by YF17D as measured by RT-qPCR (**Fig. 6a and 6b**). Consistent with cellular experiments, this block was specific to YFV and had no effect on Zika virus infection (**Fig. 6c and 6d**). These results, together with the overexpression data, confirm that the mosquito LRP8 homolog is a key factor mediating YFV infection in a natural host.

.

Purified Ectodomain of LRP8 protein blocks YFV infection

YFV infection of immunocompetent mice causes mortality when injected intracerebrally, a well-established model for assessing virulence. Using this model, we employed a decoy approach to test LRP8 function in mice. Purified Fc-tagged LRP8-LBD demonstrated dose-dependent, specific inhibition of YFV infection in U87-MG cells (**Fig. 6e**). C57BL/6 mice were injected intracerebrally with 17D preincubated with either purified Fc-tagged LRP8-LBD or an isotype IgG control. Mortality was significantly decreased in the LRP8-LBD group compared with controls (**Fig. 6f**), so are the viral loads shown by qRT-PCR and immunohistochemistry staining (**Fig. 6g and 6h**), confirming that soluble LRP8-LBD can block 17D infection and supporting its role as a receptor that directly binds YFV E on the virion surface.

Discussion

Virus receptors provide essential footholds for host-cell entry. Discovering them enables delineation of viral life cycles, interpretation of pathogenesis,

292 and development of therapies. LRP8 serving as a YFV receptor explains
293 neurotropism, while the receptor(s) responsible for viscerotropism likely
294 include additional factors. LRP8 as a YFV host factor is conserved from
295 mosquitoes and ticks to non-human primates and humans, providing a
296 consistent entry point across transmission cycles—akin to alphaviruses, which
297 are also arboviruses. This suggests an advantage to a
298 one-receptor-for-many-hosts strategy, with fewer evolutionary constraints.
299 Closest relatives of YFV such as Sepik and Wesselsbron viruses do not
300 appear to engage LRP8. Recent work also suggests that tick-borne
301 encephalitis virus (TBEV) uses LRP8, and phylogenetic analysis indicates that
302 LDLR-family usage has arisen in distant virus families, likely via independent
303 evolution (**Extended Fig. 12**). Often multiple LDLR-family members can
304 support entry for a given virus. For YFV, our data indicate that, in addition to
305 LRP8, LRP4 and VLDLR can promote entry, possibly in different cells or
306 tissues. This receptor redundancy highlights the advantage of overexpression
307 screens, which can overcome redundancy that confounds loss-of-function
308 approaches. That the soluble LRP8 LBD can block YFV infection, together
309 with prior studies, raises the possibility of LRP8-based protein therapeutics or
310 prophylactics for multiple arboviruses. Finally, wild-type YFV strains such as
311 Asibi or BJ01 do not respond to mouse LRP8 or VLDLR as robustly as 17D,
312 consistent with mice not being the natural host and suggesting adaptation to
313 mouse LRP8 during historical passaging to generate 17D. These findings
314 illuminate the evolutionary path underlying one of the most successful
315 vaccines and may inform prevention strategies for other flaviviruses.
316

317 **Acknowledgements**

318 This work was supported by a grant from the State Key Research
319 Development Program of China to X.T. (2021YFA1302503 and
320 2022YFE0102200). We thank Wang L, Ding N and Yan X for technical
321 assistance, Zhang Yuhang and Zhang Guigen for editing the manuscript.
322

323 **Author contributions**

324 X.T. conceived and supervised the project. M. M., Y. Yang, Z. Zhang, Y. Yin, J.
325 T., J. C., Y. G., Z. W., D. W., Y. J., Y.C., H. W. conducted the experiments.
326 Zhiyuan Zhang, L. L. and Y. P. contributed computational analysis, R. L., Q.
327 H., Z.D., Q. H., C. S., Y. Z J. L., W. T., L. M. and G. C. provided reagents,
328 guidance and facility support. M.M. and X.T. wrote the manuscript with input
329 from all other authors.
330

331 **Competing interests**

332 The authors declare no competing interests.

333 **Materials and Methods**

334 **Cells and viruses**

335 We maintained HEK293T (human kidney epithelial, ATCC CRL-11268),
336 HEK293FT (human kidney epithelial, Thermo Fisher Scientific, R70007),
337 U87MG (human glioblastoma, ATCC HTB-14), Vero (Cercopithecus aethiops
338 kidney, ATCC CCL-81), A549 (human lung epithelial, ATCC CCL-185), Huh7
339 (human hepatoma, CRL-10741), K562 (chronic myelogenous leukemia
340 cell line, CCL-243), C6/36 (Aedes albopictus larva, ATCC CRL-1660), and
341 BHK-21 (ATCC CCL-10) in DMEM (Gibco) supplemented with 10% fetal
342 bovine serum (FBS), Primary human hepatocytes (Shenzhen Liver
343 Biotechnology Co., Ltd.), 1% GlutaMAX (Thermo Fisher Scientific, 35050061),
344 and 1% penicillin–streptomycin (Thermo Fisher Scientific, 151401148). We
345 confirmed the absence of mycoplasma by monthly testing using myco-Lumi
346 (Beyotime, C202985S) after ZellShield treatment (Minerva Biolabs, 13-0050).
347

348 Wild-type live flaviviruses used were YFV (clinical strain BJ01、Asibi and the
349 live-attenuated vaccine strain YF17D) and ZIKV (strain SZ01). Viruses were
350 propagated in C6/36 or Vero cells and titrated in BHK-21 by plaque assay.

351 **Antibodies**

352 Reagents included: anti-YFV Env (Creative Diagnostics, CABT-YN1194), anti-
353 ZIKV Env (Creative Diagnostics, CABT-YN1207), LRP4 (Invitrogen, MA5-
354 45577), LRP4 (GeneTex, GTX637988), ApoER2/LRP8 (Santa Cruz, sc-
355 293472), Anti-VLDLR (GeneTex, GTX79552), LRP8 (Thermo Fisher, MA5-
356 38566), ApoER2/LRP8 (Abclonal, A10517), pan-flavivirus Env (Creative
357 Diagnostics, CABT-YN1131), 4G2 (Millipore, MAB10216), anti-Tim1 (Abclonal,
358 A2831 and A26862), HRP-conjugated anti-rabbit (ZSGB-Bio, ZB-2301) anti-
359 mouse (ZB-2305), and anti-human (W4038), Alexa Fluor 488 goat anti-mouse
360 (A-11001), and Alexa Fluor 568 goat anti-rabbit (A-11011).
361

362 **Reporter pseudovirus particle generation**

363 To generate replication-incompetent reporter pseudovirus particles (RPPs),
364 we used a DNA-based WNV replicon lacking the C-prM-E coding region
365 (pWNVrep dCprME-GFP) co-transfected with a plasmid expressing flaviviral
366 CprME. We cloned CprME of ZIKV strain SZ01 (GenBank KU866423), YF17D
367 (GenBank OR509732), Asibi (GenBank MF405338), CNYF01 (GenBank
368 KU921608), WESSV (GenBank NC_012735), SEPV (GenBank DQ837642),
369 Dengue virus type 2 (GenBank NC_001474), WNV (GenBank NC_001563.2),
370 JEV (GenBank NC_001437.1), and mutants into pcDNA3.1 under a CMV
371 promoter. HEK293T cells (5×10^6 per 15-cm dish) were seeded 12–18 h
372 before transfection. Standard medium (DMEM + 10% FBS, penicillin–
373 streptomycin, GlutaMAX) was used; cells were 50–60% confluent at
374 transfection. We co-transfected 30 μg pWNVrep dCprME-GFP and 10 μg

375 pcDNA3.1-CprME using Neofect reagent, replaced medium at 8 – 12 h, and
376 collected supernatants 3 days post-transfection. Supernatants were
377 centrifuged (4,000 rpm, 5 min), filtered (0.45 μm), and stored at −80 ° C.
378
379 For purification, supernatants at 48 and 72 h were clarified (4,000 rpm, 10 min)
380 and concentrated by Amicon Ultra-30 kDa units or purified on 10–60%
381 continuous sucrose gradients (200,000 g, 2 h). Bands were collected and
382 washed three times with ice-cold PBS using Amicon-30 kDa filters.
383 Preparations were stored at −80 °C (long-term) or 4 °C (≤2 weeks). Antigen
384 content was quantified by YFV ELISA (COIBIO, CB11927-Hu).

385 **Production and Purification of YF17D Live-Attenuated Virus**
386 YF17D was propagated in C6/36 at MOI 0.5 and 28 °C. Six days post-
387 infection, supernatant was harvested and centrifuged at 4,000 rpm for 30 min
388 to remove debris, filtered (0.45 μm), and precipitated with 40% PEG8000 at
389 4 °C overnight. Pellets were collected (11,000 rpm, 30 min), resuspended in
390 TNE buffer (Shyuanye R20992), and purified by ultracentrifugation on a 24%
391 sucrose cushion (105,000 g, 2 h, 4 °C). Further purification used a 10–35%
392 potassium tartrate gradient (32,000 rpm, 2 h, 4 °C). Visible bands were
393 collected and concentrated by ultrafiltration (100 kDa MWCO).

394 **VLP labelling and imaging**
395 Purified YF17D or ZIKV VLPs were labelled with Alexa Fluor 647 NHS ester in
396 0.1 M sodium bicarbonate (pH 8.3) for 30 min at room temperature in the dark.
397 Reactions were quenched with 50 mM Tris–HCl (pH 7.5), and unbound dye
398 was removed by centrifugal filtration (100 kDa MWCO). Input was normalized
399 by envelope antigen content. HEK293T cells stably expressing luciferase,
400 TIM1, LRP8-ΔLBD, or LRP8 were used. Binding assays were performed at
401 4 °C for 45 min with six PBS/2% FBS washes; internalization was at 37 °C for
402 30 min with optional proteinase K treatment (500 ng/mL, 15 min, 37 °C). Cells
403 were stained with FITC–WGA (5 μg/mL, 10 min, 4 °C) and DAPI, fixed in 4%
404 paraformaldehyde, and imaged by confocal microscopy. Single-cell VLP
405 counts were quantified using CellProfiler.
406

407 **Bio-layer interferometry analysis**
408 BLI analysis were performed at 25°C using an Octet R8 biosensor
409 system (Sartorius). YFV E antibody (GTX638626, GeneTex) was mixed and
410 incubated with biotin (#G-MM-IGT, Genemore) at a molar ratio of three biotins
411 to one protein at room temperature for 30min. Excess biotin was removed
412 using a desalting column(#G-MM-IGT, Genemore). Biotinylated protein
413 (25μg·mL^{-1}) was immobilized onto the SA Biosensors (Sartorius #18-5019) for
414 3 min and then used to capture YFV VLPs or YFV-17D viruses. The tips were
415 washed with the wash buffer (20 mM HEPES, 150 mM NaCl, pH 8.0) for 3

416 min to obtain a baseline reading, then the biosensors were dipped into wells
417 containing the LRP8-Fc at various different concentrations for the indicated
418 time. BLI data analysis was performed by using the software Octet (version
419 12.2, Sartorius) in the standard 1:1 binding mode. Raw binding data were
420 exported and plotted in GraphPad Prism8.0.
421

422 **Genome-wide ORF overexpression screen**

423 The pooled human ORF library contains 20,432 clonal ORFs mapping to
424 13,833 genes. HEK293T cells (1×10^7 per 150 mm dish) were transfected
425 with lentiviral ORF sublibraries and packaging plasmids (SV40 VSVg, Gag/Pol,
426 TAT, Rev; 1:1:1:1) using Neofect. Supernatants were collected at 36–48 h,
427 aliquoted, and stored at −80 °C. Sub-library titers were determined by
428 puromycin selection. Five million HEK293T cells were transduced at MOI 0.2,
429 selected with puromycin (2 μg/mL, 3 days), mixed in equal numbers, and
430 infected with YF17D-GFP at MOI 0.2 or mock-infected. At 24 hpi, GFP+ and
431 GFP− cells were sorted by FACS. Genomic DNA was extracted, barcodes
432 amplified, and sequenced (HiSeq-PE150). Reads were trimmed with Cutadapt,
433 aligned with Bowtie2, processed with SAMtools, counted with a custom
434 Python script, normalized with DESeq2, and log2 fold changes calculated
435 relative to GFP− samples. Scores integrated read counts and fold change
436 (see Supplementary Data Set).
437

438 **Viral entry assay**

439 For binding assays, HEK293T-Luc, HEK-LRP8iso3, U87MG-Cas9 only,
440 U87MG-sgNT, U87MG-sgLRP8-1, and U87MG-sgLRP8-2 cells (0.1 M per
441 well, 24-well plates) were incubated with YF17D, BI01 and / or Asibi at MOI 1
442 at 4 °C for 45 min and washed six times with ice-cold PBS/2% FBS. An anti-
443 YFV Env antibody (Creative Diagnostics, CABT-YN1194) served as a
444 blocking control (virus preincubated with 30× diluted antibody at 37 °C for 1 h).
445 Cells were lysed in RLT buffer (R4111, Magen) and RNA extracted for RT–
446 qPCR. For internalization, after binding and washing, prewarmed medium
447 (37 °C, 2% FBS, 15 mM NH4Cl) was added and cells were incubated for 1 h
448 at 37 °C. Residual surface virions were removed with proteinase K (500
449 ng/mL, 15 min, 37 °C) and ice-cold PBS/2% FBS before RNA extraction.
450

451 **Ectopic overexpression experiments**

452 For stable or transient expression assay, ORFs of LRP8 (GenBank
453 NM_017522.5), and LDL family: LRP3 (GenBank NM_002335.4), LRP4
454 (GenBank NM_002334.4), LRP5 (GenBank NM_002335.4), LRP6 (GenBank
455 NM_002336.3), LRP9 (GenBank NM_003105.6), LRP10 (GenBank
456 NM_014045.5), LRP11 (GenBank NM_032832.6), LRP12 (GenBank

457 NM_013437.5), LDLR (GenBank NM_000527.5), LDLRAD2 (GenBank
458 NM_001013693.3), LDLRAD3 (GenBank NM_174902.4), VLDLR (GenBank
459 NM_013703), CD209 (GenBank NM_021155.4), TIM1 (GenBank
460 NM_012206.3) were cloned into a CMV-driven lentivector with FLAG/HA tags.
461 Codon-optimized LRP1 (GenBank NM_002332), LRP2 (GenBank
462 NM_004525.3), *A. aegypti* LRP8 (GenBank XP_021711662), *Aedes*
463 *albopictus* VLDLR (GenBank XM_029869759.2), *Equus caballus* LRP8
464 (GenBank XP_023485552), *Sturnus vulgaris* LRP8 (GenBank
465 XM_014870608.1), *Canis lupus familiaris* LRP8 (GenBank XM_038666202.1),
466 *D. rodundus* bat LRP8 (GenBank XM_053920761.1), *Alligator*
467 *mississippiensis* LRP8 (GenBank XM_014598721.3), *Gallus chicken* LRP8
468 (GenBank NM_205186.3), *Ixodes scapularis* VLDLR (GenBank
469 XM_029983583.4), mouse LRP8 (GenBank NM_001369051.1), mouse
470 VLDLR (GenBank NM_013703.2), were synthesized into pcDNA3.1 with
471 C-terminal 3×HA. Lentiviral transduction and puromycin selection (2 μg/mL, 3
472 days) generated stable lines. For HA-tagged constructs, surface expression
473 was confirmed by FACS using surface staining. The target protein sequences
474 from NCBI were downloaded and performed multiple sequence alignment by
475 Clustal W using the Geneious software package.
476
477 **Genetic knockdown and knockout validation**
478 Specific siRNAs targeting LRP8 were synthesized by Jintuosi. In PHH cells
479 (Liver Biotechnology), 100nM siRNAs were transfected using RNAiMax. After
480 48 hours, the medium was replaced with PHH maintenance medium, and the
481 cells were infected with YF17D and BJ01. Another 48 hours later, the cells
482 were collected to detect viral RNA levels and the knockdown efficiency of
483 LRP8 mRNA. The siRNA sequences are as follows:
484 siLRP8-1: CCUUGAAGAUGAUGGACUATT,
485 siLRP8-2: CTGGACTGACTCGGGCAATAA.
486 The single guide RNAs targeting LRP8 (Genebank NG011517) were
487 designed as follows,
488 F1, caccgCGTCACACTTCCACCGTTCG,
489 R1, aaacCGAACGGTGGAAGTGTGACGc;
490 F2: caccgACTGTCTGCACAGGTCTTCT,
491 R2: aaacAGAAGACCTGTGCAGACAGTc). Then these guide RNAs were
492 cloned into lenti-CRISPRv2 plasmid (Addgen#52961). Lentivirus was
493 collected from the supernatant of HEK293T cells transfected with lenti-
494 CRISPRv2 in addition of packaging plasmids aforementioned. LRP8 knockout
495 (KO) clones were generated by single guide RNA in U87MG and selected
496 with 2 μg/mL puromycin for 5-7 days. Further sgLRP8 cells were pooled in 96-
497 well plates at a density of 0.5 cell per well to obtain single-cell clones. Each
498 clone was validated by Western blot or Sanger sequencing.

499

500 **Pull-down assay**

501 Purified soluble LRP8-Fc (10 μg) or isotype IgG was incubated with 30 μL
502 protein A/G magnetic beads (Thermo Fisher Scientific) in PBS/0.1%
503 Tween-20 at 4 °C for 6 h. After removing unbound proteins, beads were
504 incubated overnight at 4 °C with clarified lysates from YF17D-infected Vero
505 cells, washed eight times with PBS/0.1% Tween-20, and eluted by boiling in
506 SDS-PAGE buffer for immunoblotting.

507

508 **Protein purification**

509 LRP8 LA1237 DNA was inserted into a vector encoding a C-terminal human
510 IgG Fc fusion and transfected into HEK293F (3.0×10^6 cells/mL).
511 Supernatants (60h after transfection) were purified on Protein A Sepharose
512 4B, washed with 20 mM HEPES/150 mM NaCl (pH 8.0), and eluted with 20
513 mM HEPES/150 mM NaCl/0.1 M glycine (pH 2.8), followed by SEC (Superdex
514 200 10/300 GL) in 20 mM HEPES/150 mM NaCl (pH 8.0). LDLR-Fc was
515 purified similarly. For VLDLR LA1-8, co-transfection with RAP enabled
516 on-column Ca2+-dependent refolding after extensive EDTA washes.
517

518 **Decoy protein and antibody-mediated blocking assay**

519 Purified LRP8-Fc (200 μg/μL stock) or isotype IgG was serially diluted,
520 preincubated with YF17D or ZIKV (pseudovirus or live) at 37 °C for 1 h, then
521 added to cells. For pseudovirus, GFP+ cells were quantified at 24 h by
522 high-content imaging. For live virus, cells were fixed at 48 h and stained with
523 4G2 and fluorescent secondary antibodies. For antibody blocking, anti-LRP8
524 or isotype controls were incubated with cells for 1 h at 37 °C before infection.
525

526 **Immunoblotting**

527 Cells and tissue samples were lysed in 1% NP-40 buffer on ice. Protein
528 concentrations were determined by BCA, samples denatured in 5×
529 SDS-PAGE buffer (10 min, 95 °C), resolved by SDS-PAGE, transferred to
530 nitrocellulose, blocked in TBST/5% milk, incubated with primary antibody
531 overnight (4 °C), washed, and probed with HRP-secondary antibodies for 1 h
532 before detection.
533

534 **Immunofluorescence**

535 Eight thousand HEK293T or U87MG cells per well in 96-well plates were
536 infected with YF17D (MOI 0.3) or ZIKV SZ01 (MOI 0.2) for 24–48 h, fixed in
537 4% paraformaldehyde, permeabilized with 0.2% Triton X-100 (Promega), and

538 stained with 4G2 (1:1000) and Alexa Fluor 488 secondary (Invitrogen,
539 R37120, 1: 1000). Nuclei were counterstained with DAPI (Invitrogen, 62247,
540 1:10,000). Images were acquired on a high-content microscope (Cytation 1)
541 and infection ratios quantified.
542

543 **Flow cytometry**

544 For membrane protein expression, cells were detached with 10 μM EDTA,
545 stained with anti-LRP8、anti-TIM1 or anti-HA for 30 min at room temperature,
546 washed, stained with AF-488 secondary for 1 h, fixed in 2%
547 paraformaldehyde, washed, and analyzed by flow cytometry. GFP+ cell ratios
548 were quantified after trypsinization for reporter assays.
549

550 **Quantitative real-time PCR**

551 DNA/RNA were extracted (Magen, R5111). Two micrograms of total RNA
552 were reverse-transcribed (ABM, G492). qPCR was performed with 2× ChamQ
553 SYBR reagents (Vazyme, Q321) on a Bio-Rad CFX96. qRT-PCR data were
554 normalized to GAPDH. The primer sets were as follows:
555 *GAPDH*-qF: CGGAGTCAACGGATTTGGTCGTAT;
556 *GAPDH*-qF: AGCCTTCTCCATGGTGGTGAAGAC;
557 *YF17D*-qF: ATGGCAGGAGGATTGTGGTG;
558 *YF17D*-qR: GTTGTGCGTCCTTGTGGAAC;
559 YFV BJ01-qF: GCTAATTGAGGTGYATTGGTCTGC;
560 YFV-BJ01-qR: CTGCTAATCGCTCAAMGAACG;
561 *YFV-Asibi*-qF*: GCACGGATGTAACAGACTGAAGA;*
562 *YFV-Asibi*-qR*: CCAGGCCGAACCTGTCAT;*
563 *LRP8*-qF: CCCATCCCTAATCTTCACCAAC;
564 *LRP8*-qR: CTAGTGCCACGACATTCTTGAG.
565

566 **In vivo mosquito experiments**

567 Four dsRNAs targeting the common region of Aedes aegypti VLDLR
568 (LOC5576021) and controls (luciferase, GFP) were designed (SnapDragon),
569 synthesized by in vitro transcription (MEGAscript, Ambion), and purified.
570 Female mosquitoes were chilled on ice and injected (1 μg/300 nl) into the
571 thorax. Gene silencing was verified by qRT-PCR. For infection, 1000 MID50
572 of YF17D or ZIKV was microinjected. Mosquitoes were collected at 4 dpi for
573 RT-qPCR.

574 Six pairs primers were synthysized as follows:
575 DS1 F: TAATACGACTCACTATAGGGATCCCCGTGATCATACCAAA
576 DS1 R: TAATACGACTCACTATAGGGCCAGTCCGTCCAGTACATCC

577 DS2 F: TAATACGACTCACTATAGGGAAACCTGCAGATCGGATGAG
578 DS2 R: TAATACGACTCACTATAGGGTTTTGCACTGGAACTGATCG
579 DS3 F: TAATACGACTCACTATAGGGCCTGCAGATCGGATGAGTTT
580 DS3 R: TAATACGACTCACTATAGGGGCAGGTTTTGTCCTTTTTGC
581 DS4 F:TAATACGACTCACTATAGGGGTATGCCGGGTTACCTGAGA
582 DS4 R: TAATACGACTCACTATAGGGTCAGAATCTTGCCCATGTTG
583 Ds-Luc-F: TAATACGACTCACTATAGGGGGACTTGGACACCGGTAAGA
584 Ds-Luc-R: TAATACGACTCACTATAGGGGTCCACGAACACAACACCAC
585 DS-GFP-F:TAATACGACTCACTATAGGGGTGAGCAAGGGCGAGGAG
586 DS-GFP-R:
587 TAATACGACTCACTATAGGGCATGATATAGACGTTGTGGCTGTT.

588

589 **Mouse infection experiment**

590 Five-week-old C57BL/6 mice were anesthetized and secured in a stereotaxic
591 apparatus. For in vivo neutralization, YF17D was premixed with purified
592 soluble LRP8-LBD-Fc or isotype IgG at 37℃ for 1 hours, each group contain
593 six equal gender mice. Ten microliter (200 PFU) was injected into the lateral
594 ventricle (AP +0.2 mm, ML ±1.0 mm, DV −2.0 mm) at 10–20 nL/s. The needle
595 was left in place for 5–10 min to minimize backflow, and incisions were closed.
596 Meloxicam (4 mg/kg, s.c.) was administered for three days. Survival was
597 monitored daily. For viral quantification in brain infection and blood, another
598 independant assay was performed, and all the mice were sacrificed at 10
599 days post infection, the blood and brain were collected.

600 In the AAV mouse model, 21 three-week-old AG129 mice were evenly divided
601 into three groups, with equal numbers of males and females. Each mouse
602 received a tail vein injection of 2×10^{11} gc of AAV2/8-TBG-LRP8, AAV2/8-TBG-
603 LDLR, or an AAV2/8-TBG empty vector, packaged by CIBR Vector Core.
604 Three weeks after AAV delivery, one mouse from each group was sacrificed
605 to examine receptor expression in the liver. After confirming successful
606 expression, each mouse was intraperitoneally injected with 10,000 PFU of
607 BJ01, then weighed daily and monitored for health status. On the fifth day
608 after YFV infection, blood was collected via the orbital vein to assess viremia,
609 liver function markers, and inflammatory factors. When the mice were close to
610 death, liver and brain tissues were collected to evaluate tissue viral titers and
611 pathological changes. All animal procedures were Tsinghua or Shenzhen
612 Third Hospital IACUC-approved and complied with institutional and national
613 guidelines.

614

615 **Sera biochemistry analysis & ELISA analysis**

616 Alanine transaminase (ALT), Aspartate aminotransferase (AST) and Total
617 Bilirubin (TBIL) in mouse serum was detected using biochemistry assay kits
618 according to the corresponding instructions. All of the reagent kits were
619 manufactured by Nanjing Jian cheng Biotechnology Co., Ltd. The levels of
620 and MCP-1 in mouse serum were measured using commercial ELISA kits
621 manufactured by Sino Biological Biotechnology Co., Ltd.
622 ALT detection kit (C009-2-1, Nanjing Jiancheng Bioengineering Institute
623 Co., Ltd)
624 AST detection kit (C010-2-1, Nanjing Jiancheng Bioengineering Institute
625 Co., Ltd)
626 TBIL detection kit (C019-1-1, Nanjing Jiancheng Bioengineering Institute
627 Co., Ltd)
628 MCP-1 ELISA kit (KIT50368, Sino Biological Biotechnology Co., Ltd).

629

630 **Immunohistochemistry**

631 After mouse sacrificed, the tissues were fixed in 4% paraformaldehyde
632 overnight at 4°C, then followed by 20%, 30% sucrose gradient dehydrated 1
633 day, embedded in OCT (SAKURA, 4583) and cut into 10 μm sections. For
634 Immunohistochemistry (IHC), antigen retrieval was performed by boiling in
635 0.01 M citrate buffer (pH 6.0) for 10 min. Endogenous hydrogen peroxidase
636 activity was blocked by 3% hydrogen peroxide in PBS for 30 min, followed by
637 incubating in primary antibodies overnight at 4 ℃, HRP-conjugated anti-rabbit
638 secondary antibody at RT (room temperature). DAB staining followed
639 instructions from the DAB detection kit (ZSGB-Bio, ZLI-9019) for 5–10 min at
640 RT, finally counter staining was performed using hematoxylin solution
641 (Solarbio, H8070). Primary antibodies and dilution factors are listed below:
642 anti-YFV Env (Creative Diagnostics, CABT-YN1194, 1:100), anti-LRP4
643 (GeneTex, GTX637988, 1:100), anti-VLDLR (Abcam, ab302917, 1:100),
644 LRP8 (Thermo Fisher, MA5-38566, 1:100), anti-LRP8 (Abclonal, A10517,
645 1:50).

646

647 **Plaque assay for viral titer identification**

648 Supernatant titration (in PFU mL−1) of each HEK293T over-expressing cells
649 was obtained by plaque assay to determine the amount of infectious viral
650 particles (PFU). The virus titration was performed in BHK21 cells, and in
651 DMEM medium with 2% FBS. Briefly, 0.25× 10^6/mL BHK21 cells were seeded
652 in each well of a 12-well plate for 12h at 37°C to allow BHK21 cell adherence.
653 Then, a serial dilution of each virus stock from YFV subculture in DMEM
654 medium (without FBS, 1% penicillin/streptomycin, and 1% glutamine) was

655 performed from 10^{-1} to 10^{-7}. Then, 400 μL of each dilution was added in each
656 well for virus adsorption 1-2hr. After this, the virus was discarded and each
657 well was overlaid with 4mL 2% DMEM media containing final 0.8% complete
658 LMP agarose. After 5 days of incubation at 37°C, the plaque visualization was
659 made using 4% PFA fixation and 0.2% crystal violet in 20% ethanol staining to
660 visualize the plaques.

661

662 **Human liver and brain tissue collection**

663 Human liver tissue used in this study was collected from a patient who
664 underwent surgical resection for hepatic hemangioma. Human brain tissue
665 used in this study was collected from the unaffected area of a brain of a
666 patient who died of epilepsy. The collection protocol was approved by the
667 Institutional Review Board of Beijing Chao-Yang Hospital, Capital Medical
668 University, and written informed consent regarding tissue donation was
669 obtained from the patient and family before surgery.

670

671 **Human liver cell suspension preparation**

672 The tissue sample was minced into small pieces and incubated in digestion
673 buffer containing 1× PBS, collagenase D (1 mg ml−1, Sigma-Aldrich), dispase
674 (2.4 mg ml−1, Thermo Fisher Scien- tific), DNase (0.2 mg ml−1, Sigma-
675 Aldrich) and 3% heat-inactivated fetal bovine serum (FBS, Invitrogen) for 30
676 min at 37 °C. Cells suspensions were dissociated and passed through a 100
677 μm cell strainer (BD).

678

679 **Cell preparation for scRNA-seq**

680 Thaw the cryovial containing frozen human liver single cells at 37℃, then
681 transfer suspension to a centrifuge tube with RPMI1640 (Gibco
682 11875119)+10% FBS(Gibco 10100147C), centrifuged for 5 min at 300×g at
683 4°C. The cells were resuspended in RPMI1640+2% FBS. Cell count and
684 viability was estimated using SeekMate Tinitan Fluorescence Cell Counter
685 (SeekGene M002C) with AO/PI reagent after removal erythrocytes (Solarbio
686 R1010) and then debris and dead cells removal was decided to be performed
687 or not (Miltenyi 130-109-398/130-090-101). Finally fresh cells were washed
688 twice in the RPMI1640 and then resuspended at 1×106 cells per ml in
689 RPMI1640 and 2% FBS.

690

691 **Single cell RNA-seq library construction and sequencing**

692 Single-cell RNA-Seq libraries were prepared using SeekOne® DD Single Cell
693 3' library preparation kit (SeekGene Catalog No.K00202). Briefly, appropriate
694 number of cells were mixed with reverse transcription reagent and then added
695 to the sample well in SeekOne® chip S3. Subsequently, Barcoded Hydrogel
696 Beads (BHBs) and partitioning oil were dispensed into corresponding wells
697 separately in chip S3. After emulsion droplet generation reverse transcription
698 were performed at 42℃ for 90 minutes and inactivated at 85℃ for 5 minutes.
699 Next, cDNA was purified from broken droplet and amplified in PCR reaction.
700 The amplified cDNA product was then cleaned, fragmented, end repaired, A-
701 tailed and ligated to sequencing adaptor. Finally, the indexed PCR were
702 performed to amplified the DNA representing 3' polyA part of expressing
703 genes which also contained Cell Barcode and Unique Molecular Index. The
704 indexed sequencing libraries were cleanup with VAHTS DNA Clean Beads
705 (Vazyme N411-01), analyzed by Qubit (Thermo Fisher Scientific Q33226) and
706 Bio-Fragment Analyzer (Bioptic Qsep400). The libraries were then sequenced
707 on GeneMind SURFSeq 5000 with PE150 read length.

708

709 **Single cell RNA-seq data analysis**

710 scRNA-seq data processing and analysis were conducted using Seurat
711 (v5.3.0). Quality control was applied by retaining cells that met the following
712 criteria: nFeature_RNA between 200 and 5000, nCount_RNA below 20000,
713 and mitochondrial gene content less than 10%. This filtering step resulted in a
714 total of 8271 cells. The data were subsequently normalized and scaled using
715 the standard Seurat workflow. Expression values of the genes of interest were
716 then extracted to generate visualizations and compute mean expression
717 levels.

718

719 **Data availability**

720 ScRNA-seq raw data have been deposited in the Genome Sequence Archive
721 (Genomics, Proteomics & Bioinformatics 2021) in National Genomics Data
722 Center, China National Center for Bioinformation / Beijing Institute of
723 Genomics, Chinese Academy of Sciences (GSA-Human: HRA013453).

724

725 **Statistical analysis**

726 Unless otherwise specified, experiments were repeated at least three times.
727 Bar graphs show mean ± SEM. Unpaired two- tailed t- tests were used for
728 p- values unless otherwise noted.
729

730

731 ## References

732 1 Bres, P. A century of progress in combating yellow fever. Bulletin of the World
733 Health Organization 64, 775-786 (1986).

734 2 Wax, R. G. Manipulation of Human History by Microbes. Clinical Microbiology
735 Newsletter 29, 9-16 (2007).

736 3 Staples, J. E. & Monath, T. P. Yellow fever: 100 years of discovery. Jama-Journal of
737 the American Medical Association 300, 960-962, doi:DOI 10.1001/jama.300.8.960
738 (2008).

739 4 Walter R, C. J., Agramonte A. The Etiology of Yellow Fever: An Additional Note.
740 Jama-Journal of the American Medical Association 36, 431-440 (1901).

741 5 Barrett, A. D. T. & Higgs, S. Yellow fever: A disease that has yet to be conquered.
742 Annu Rev Entomol 52, 209-229, doi:10.1146/annurev.ento.52.110405.091454
743 (2007).

744 6 Yellow fever, <https://www.who.int/news-room/fact-sheets/detail/yellow-fever>
745 (2023).

746 7 Hansen, C. A. & Barrett, A. D. T. The Present and Future of Yellow Fever Vaccines.
747 Pharmaceuticals-Base 14, doi:ARTN 891 10.3390/ph14090891 (2021).

748 8 Meier, K. C., Gardner, C. L., Khoretonenko, M. V., Klimstra, W. B. & Ryman, K. D. A
749 Mouse Model for Studying Viscerotropic Disease Caused by Yellow Fever Virus
750 Infection. Plos Pathog 5, doi:ARTN e1000614 10.1371/journal.ppat.1000614 (2009).

751 9 Vasconcelos, P. F. C. & Monath, T. P. Yellow Fever Remains a Potential Threat to
752 Public Health. Vector-Borne Zoonot 16, 566-567, doi:10.1089/vbz.2016.2031 (2016).

753 10 Orenstein, W. A., Offit, P. A., Edwards, K. M. & Plotkin, S. A. Plotkin's vaccines. 8th
754 edition. edn, (Elsevier, 2024).

755 11 Wang, H. J. et al. Development of a Bicistronic Yellow Fever Live Attenuated
756 Vaccine with Reduced Neurovirulence and Viscerotropism. Microbiol Spectr 10,
757 doi:10.1128/spectrum.02246-22 (2022).

758 12 Davis, E. H. et al. Impact of yellow fever virus envelope protein on wild-type and
759 vaccine epitopes and tissue tropism. Npj Vaccines 7, doi:ARTN 39 10.1038/s41541-
760 022-00460-6 (2022).

761 13 Lee, E. & Lobigs, M. E protein domain III determinants of yellow fever virus 17D
762 vaccine strain enhance binding to glycosaminoglycans, impede virus spread, and
763 attenuate virulence. J Virol 82, 6024-6033, doi:10.1128/Jvi.02509-07 (2008).

764 14 Zhang, J. Y. et al. Amino acid changes in two viral proteins drive attenuation of the
765 yellow fever 17D vaccine. Nat Microbiol 10, doi:10.1038/s41564-025-02047-y (2025).

766 15 Nickells, J. et al. Neuroadapted Yellow Fever Virus Strain 17D: a Charged Locus in
767 Domain III of the E Protein Governs Heparin Binding Activity and Neuroinvasiveness
768 in the SCID Mouse Model. J Virol 82, 12510-12519, doi:10.1128/Jvi.00458-08 (2008).

769 16 Fernandez-Garcia, M. D. et al. Vaccine and Wild-Type Strains of Yellow Fever Virus
770 Engage Distinct Entry Mechanisms and Differentially Stimulate Antiviral Immune
771 Responses. Mbio 7, doi:ARTN e01956-15 10.1128/mBio.01956-15 (2016).

772 17 Douam, F. & Ploss, A. Yellow Fever Virus: Knowledge Gaps Impeding the Fight
773 Against an Old Foe. Trends Microbiol 26, 913-928, doi:10.1016/j.tim.2018.05.012
774 (2018).

775 18 Sack, L. M. et al. Profound Tissue Specificity in Proliferation Control Underlies
776 Cancer Drivers and Aneuploidy Patterns. Cell 173, 499-+, doi:ARTN 514.e1
777 10.1016/j.cell.2018.02.037 (2018).

778 19 Li, S. et al. Gain-of-function genetic screening identifies the antiviral function of
779 TMEM120A via STING activation. Nat Commun 13, 105, doi:10.1038/s41467-021-
780 27670-1 (2022).

781 20 Pierson, T. C. et al. A rapid and quantitative assay for measuring antibody-mediated
782 neutralization of West Nile virus infection. Virology 346, 53-65,
783 doi:10.1016/j.virol.2005.10.030 (2006).

784 21 Herz, J. The LDL receptor gene family: (Un)expected signal transducers in the brain.
785 Neuron 29, 571-581, doi:Doi 10.1016/S0896-6273(01)00234-3 (2001).

786 22 Kim, D. H. et al. Human apolipoprotein E receptor 2 - A novel lipoprotein receptor of
787 the low density lipoprotein receptor family predominantly expressed in brain. J Biol
788 Chem 271, 8373-8380, doi:DOI 10.1074/jbc.271.14.8373 (1996).

789 23 Novak, S., Hiesberger, T., Schneider, W. J. & Nimpf, J. A new low density lipoprotein
790 receptor homologue with 8 ligand binding repeats in brain of chicken and mouse (vol
791 271, pg 11732, 1996). J Biol Chem 271, 27188-27188 (1996).

792 24 Clark, L. E. et al. VLDLR and ApoER2 are receptors for multiple alphaviruses.
793 Nature 602, 475-+, doi:10.1038/s41586-021-04326-0 (2022).

794 25 Meertens, L. et al. The TIM and TAM Families of Phosphatidylserine Receptors
795 Mediate Dengue Virus Entry. Cell Host Microbe 12, 544-557,
796 doi:10.1016/j.chom.2012.08.009 (2012).

797 26 Hirai, H. et al. Structural basis for ligand capture and release by the endocytic
798 receptor ApoER2. Embo Rep 18, 982-999, doi:10.15252/embr.201643521 (2017).

27 Li, M. et al. Rift Valley Fever Virus and Yellow Fever Virus in Urine: A Potential Source of Infection. Virol Sin 34, 342-345, doi:10.1007/s12250-019-00096-2 (2019).

28 Pierson, T. C., Lazear H.M., Diamond M.S. in Fields Virology Vol. 1 (ed P.M. Howley, Knipe, D.M.) Ch. 9, volumes (Wolters Kluwer, 2021).

Figure legends

Figure 1. Human genome-wide ORFeome library screening identifies LRP8 as a YFV receptor. **a,** Schematic of the workflow of the screen. **b,** Deep-sequencing analysis of the screen performed with YF17D-GFP in HEK293T cells stably expressing the human ORFeome library. The x-axis shows log2 fold change of a gene's read counts in GFP+ versus GFP− cells; the y-axis shows −log10 p-values. **c-e,** Luciferase, LDLR, LRP8, or TIM1 were expressed in HEK293T cells and infected with YF17D, ZIKV, Dengue virus 2, WNV, JEV, SEPV or WESSV pseudoviruses. Blue and green indicate DAPI and GFP, respectively. **d**, Quantification of **c**. **e**, Supernatants from HEK293T overexpressing luciferase or LRP8 infected by live YF17D virus at 48 hpi were collected and the viral titers were determined using palque assay in BHK21 cells. **f-g**, Ectopic LRP8 expression enhanced infection of YF17D (MOI 0.1) (**e**) and BJ01 (MOI 0.01) (**f**) shown in a time course. Viral RNA was normalized to GAPDH. h. HEK293T cells were transfected with the indicated genes were infected with the indicated pseudoviruses for 48h before being analyzed by FACS. The statistics shown are Mean ± SEM. *: $P < 0.05$; **: $P < 0.01$; ***: $P < 0.001$; ****: $P < 0.0001$ (unpaired two-sided t-test). The replicate in the figure indicates biological replicates, the experiments were repeated at least three times.

Figure 2. YFV infection requires LRP8 in U87-MG cells. **a**, Cas9/sgRNAs or Cas9 only were expressed in U87MG; single clones were selected. Knockout cells were infected with 17D-GFP for two days and analyzed by Western blot. sgNT: non-targeting sgRNA; sgLRP8-1/2: sgRNAs targeting human LRP8. **b–c**, LRP8 knockout cells or control cells were infected with live 17D or ZIKV for two days, fixed, stained with 4G2 and DAPI, imaged, and quantified. **d-e**, Knockout cells were infected with the clinical BJ01 and Asibi strain, viral RNA was quantified by RT–qPCR. **f–h**, U87MG LRP8-KO cells were reconstituted with LRP8 WT or LRP8-ΔLBD by electroporation and infected with 17D-GFP or ZIKV-GFP; imaging and quantification as above. **h**, Western blot analysis of LRP8 and GFP as in the 17D-GFP infected group of **f**. **i**, U87MG cells pretreated with an anti-LRP8 antibody or isotype IgG were infected with YF17D or ZIKV and quantified by 4G2 staining. The statistics shown are Mean ± SEM. *: $P < 0.05$; **: $P < 0.01$; ***: $P < 0.001$; ****: $P < 0.0001$

840 (unpaired two-sided t-test). The replicate in the figure indicates biological
841 replicates, the experiments were repeated at least three times.
842
843 **Figure 3**. LRP8 promotes YFV entry by binding to its envelope protein. **a**,
844 HEK293T cells stably expressing luciferase or LRP8 were infected with
845 YF17D at MOI 1 either at 4 °C for 45 min to measure binding or at 37 °C for 1
846 h to measure internalization. **b–c**, U87MG LRP8-KO and Cas9-only control
847 cells were tested similarly; a pan-flavivirus E antibody served as a blocking
848 control. **d–f**, HEK293T cells expressing LRP8, LRP8-ΔLBD, TIM1, or
849 luciferase were treated with Alexa Fluor 647–labeled VLPs bearing YFV 17D
850 E (**d, e**) or ZIKV E (**f**). FITC–WGA was added to label cell membranes before
851 imaging. **g**, Pulldown of YF17D E protein by immobilized LRP8 LBD-Fc. **h, i,**
852 BLI measurement of immobilized live YF17D (**h**) or YF17D VLP (**i**) binding to
853 soluble LRP8-LBD. The statistics shown are Mean ± SEM. *: P < 0.05; **: P <
854 0.01; ***: P < 0.001; ****: P < 0.0001 (unpaired two-sided t-test). The replicate
855 in the figure indicates biological replicates, the experiments were repeated at
856 least three times.
857
858 **Figure 4**. Effects of LDLR family members and LRP8 homologs on YFV
859 infection. **a, b, c**, HEK293T cells transfected with LDLR family members were
860 infected with YF17D-GFP or BJ01 or Asibi for 48 h and analyzed by
861 fluorescence microscopy (YF17D-GFP) or qRT-PCR (BJ01 and Asibi). **d**, **e**,
862 LRP8 homologs from different species were expressed in HEK293T cells and
863 infected with YF17D-GFP or BJ01 for 48 h and analyzed by fluorescence
864 microscopy (YF17D-GFP) or qRT-PCR (BJ01). The statistics shown are Mean
865 ± SEM. *: P < 0.05; **: P < 0.01; ***: P < 0.001; ****: P < 0.0001 (unpaired
866 two-sided t-test). The replicate in the figure indicates biological replicates, the
867 experiments were repeated at least three times.
868
869 **Figure 5**. LRP8 is expressed in human liver and mediates YFV infection in
870 primary human hepatocytes and in a mouse model. **a**, LRP8, LRP4 and
871 VLDLR expression were determined in human brain or liver by
872 immunohistochemistry staining with corresponding antibodies. **b**, Scaled
873 expression levels of LRP8, LRP4 and VLDLR in human liver single cell
874 RNAseq data. The red dot within each column represents the mean
875 expression value across all cells. **c**, Western blots of human liver samples,
876 including crude liver lysates, showed clear LRP8 expression at levels
877 comparable to brain. HEK293T cells overexpressing one of the three genes
878 were included as controls showing the specificity of the antibodies. **d-i**,
879 Primary human hepatocytes were transfected with siRNAs targeting LRP8 or
880 non-targeting control siRNAs (NC-1 and NC-2) for 48 hours and infected with
881 live YF17D (**d-f**) or BJ01 (**g, i**) for 48 hour, and the viral RNA and LRP8

882 mRNA level from cell total RNA were quantified via qRT-PCR (**d, f, g, j**). The
883 virus titers of the supernatant were quantified by plaque assay (**e, h**). **j-p**, In
884 AG129 mice, 2x 10^{11} genome-copies of AAV-TBG expressing either LRP8 or
885 LDLR and an empty AAV were injected by tail vein into each mouse. Three
886 weeks later, YFV BJ01 was injected intraperitoneally. The survival curve of
887 the mice were shown in j. Five days post YFV injection, the blood was drawn
888 from the mice to measure viral load (**k**) and levels of ALT and AST enzymatic
889 activities and levels of bilirubin and MCP-1 (**i-o**). The livers of a mock mouse
890 and two mice each from the LDLR and LRP8 group died at day 7 (LRP8
891 group) or day 10 (LDLR group) were processed for immunohistochemistry
892 imaging with DAB staining of YFV E protein with an anti-E antibody, asterisks
893 indicate sites of positive staining (**p**). The statistics shown are Mean ± SEM. *:
894 P < 0.05; **: P < 0.01; ***: P < 0.001; ****: P < 0.0001 (unpaired two-sided t-
895 test). The replicate in the figure indicates biological replicates, the
896 experiments were repeated at least twice.
897
898 **Figure 6**. LRP8 function in YFV infection in animal models. **a–b**, *Aedes*
899 *aegypti* mosquitoes injected with dsRNA targeting VLDLR or control dsRNA
900 for three days were then infected with YF17D. Four days post infection, viral
901 RNA (**a**) and VLDLR mRNA (**b**) were quantified by qRT–qPCR. **c–d**, dsRNA-
902 treated mosquitoes were infected with ZIKV. **e**, YF17D or 17D-GFP was
903 treated with soluble LRP8 LBD-Fc or isotype IgG and used to infect U87MG
904 cells; infection was quantified by immunofluorescence or GFP. **f**, C57BL/6
905 mice were injected intracerebrally with YF17D preincubated with LRP8 LBD-
906 Fc or isotype IgG; survival was recorded daily. **g**. Brain from mice of **f** was
907 drawn to measure viral load by qRT-PCR. **h**. In a repeat experiment of **f**. mice
908 at day 10 post infection were sacrificed and the brain of the mice were
909 processed for immunohistochemistry imaging with DAB staining of YFV E
910 protein with an anti-E antibody. The statistics shown are Mean ± SEM. *: P <
911 0.05; **: P < 0.01; ***: P < 0.001; ****: P < 0.0001 (unpaired two-sided t-test).
912 The replicate in the figure indicates biological replicates, the experiments
913 were repeated at least twice.
914
915
916
917

Fig.1

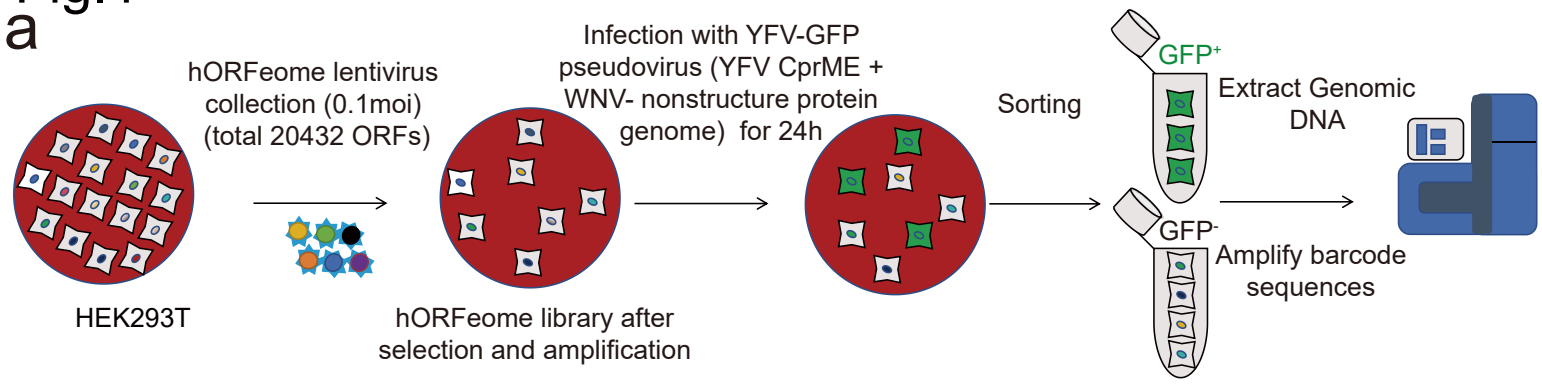
a
hORFeome lentivirus collection (0.1moi) (total 20432 ORFs)
Infection with YFV-GFP pseudovirus (YFV CprME + WNV- nonstructure protein genome) for 24h
Sorting
GFP+
GFP-
Extract Genomic DNA
Amplify barcode sequences
HEK293T
hORFeome library after selection and amplification

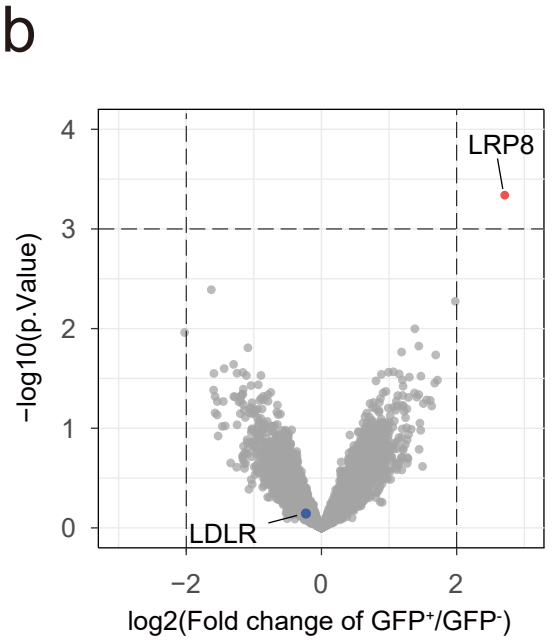
b
LRP8
LDLR
−log10(p.Value)
log2(Fold change of GFP+/GFP-)

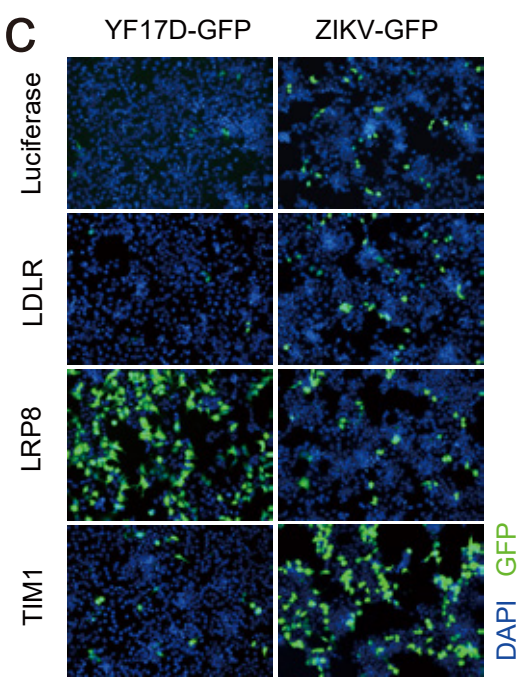
c
YF17D-GFP
ZIKV-GFP
Luciferase
LDLR
LRP8
TIM1
GFP
DAPI

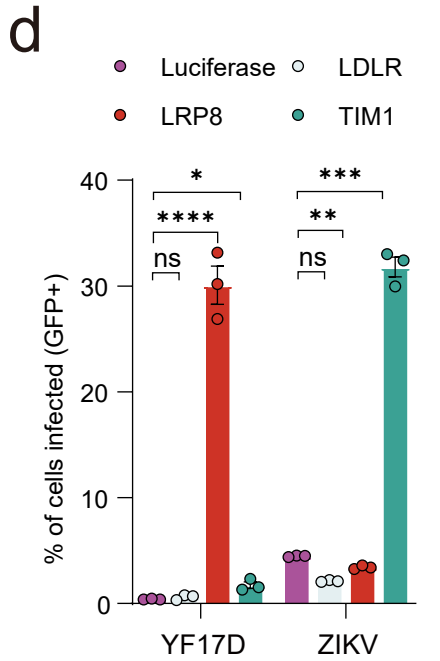
d
Luciferase
LDLR
LRP8
TIM1
% of cells infected (GFP+)
ns
****
*
ns
**
***
YF17D
ZIKV

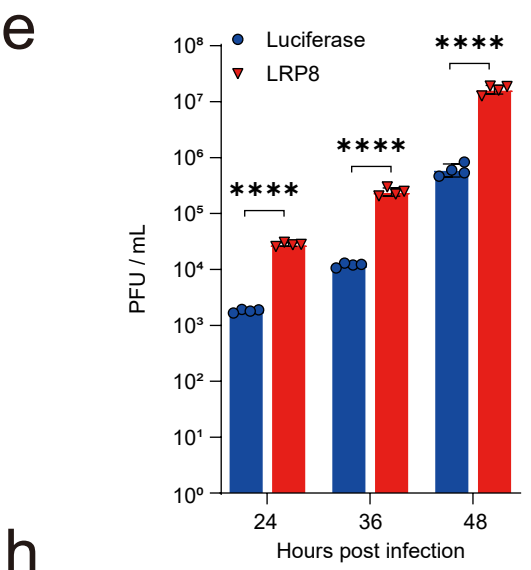
e
Luciferase
LRP8
PFU / mL
****
****
****
Hours post infection

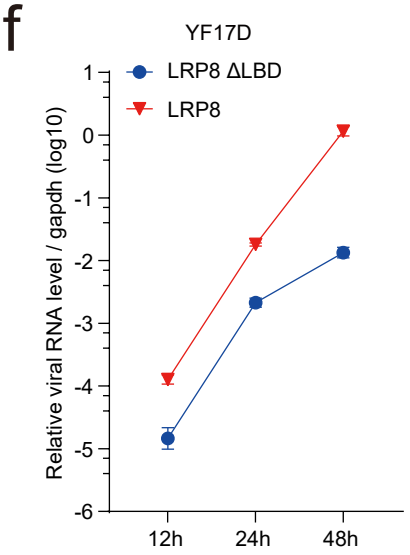
f
YF17D
LRP8 ΔLBD
LRP8
Relative viral RNA level / gapdh (log10)
12h
24h
48h

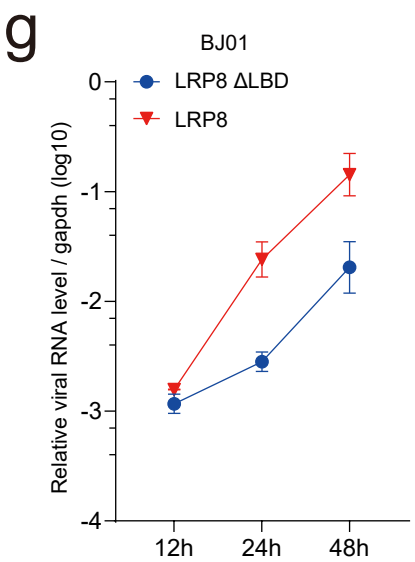
g
BJ01
LRP8 ΔLBD
LRP8
Relative viral RNA level / gapdh (log10)
12h
24h
48h

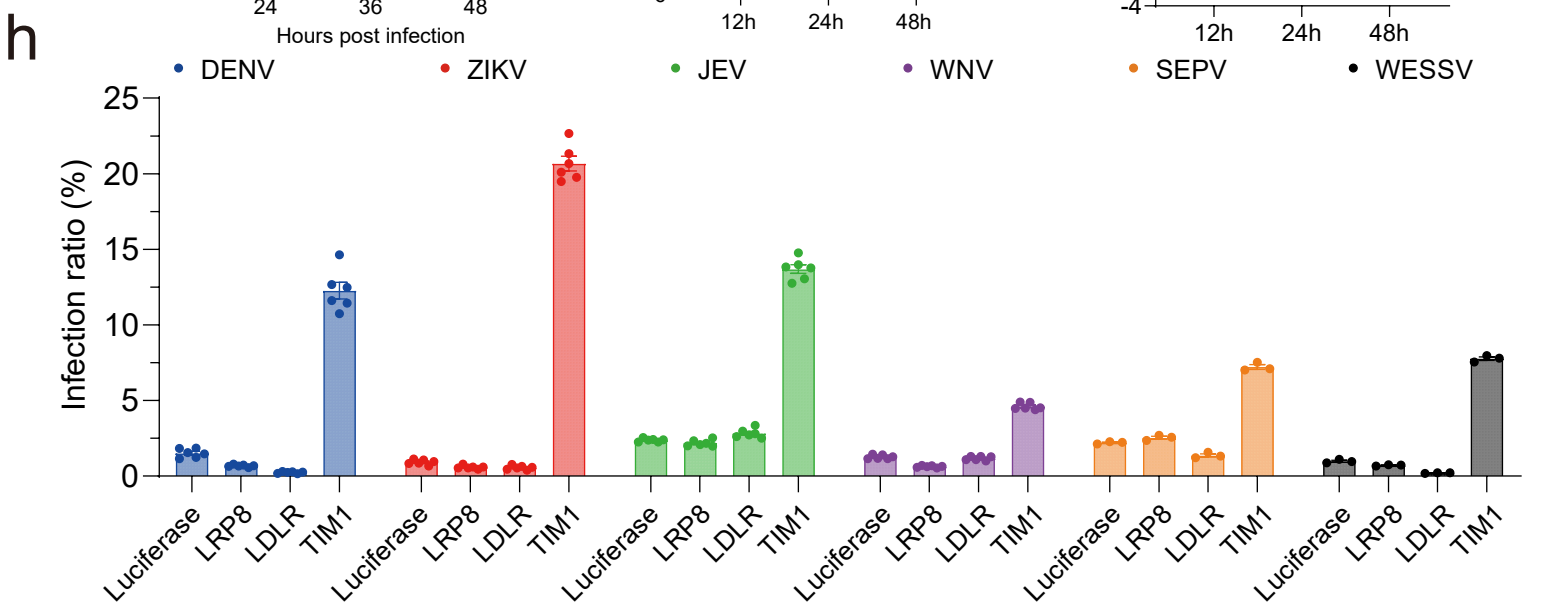
h
DENV
ZIKV
JEV
WNV
SEPV
WESSV
Infection ratio (%)
Luciferase
LRP8
LDLR
TIM1

Fig.2

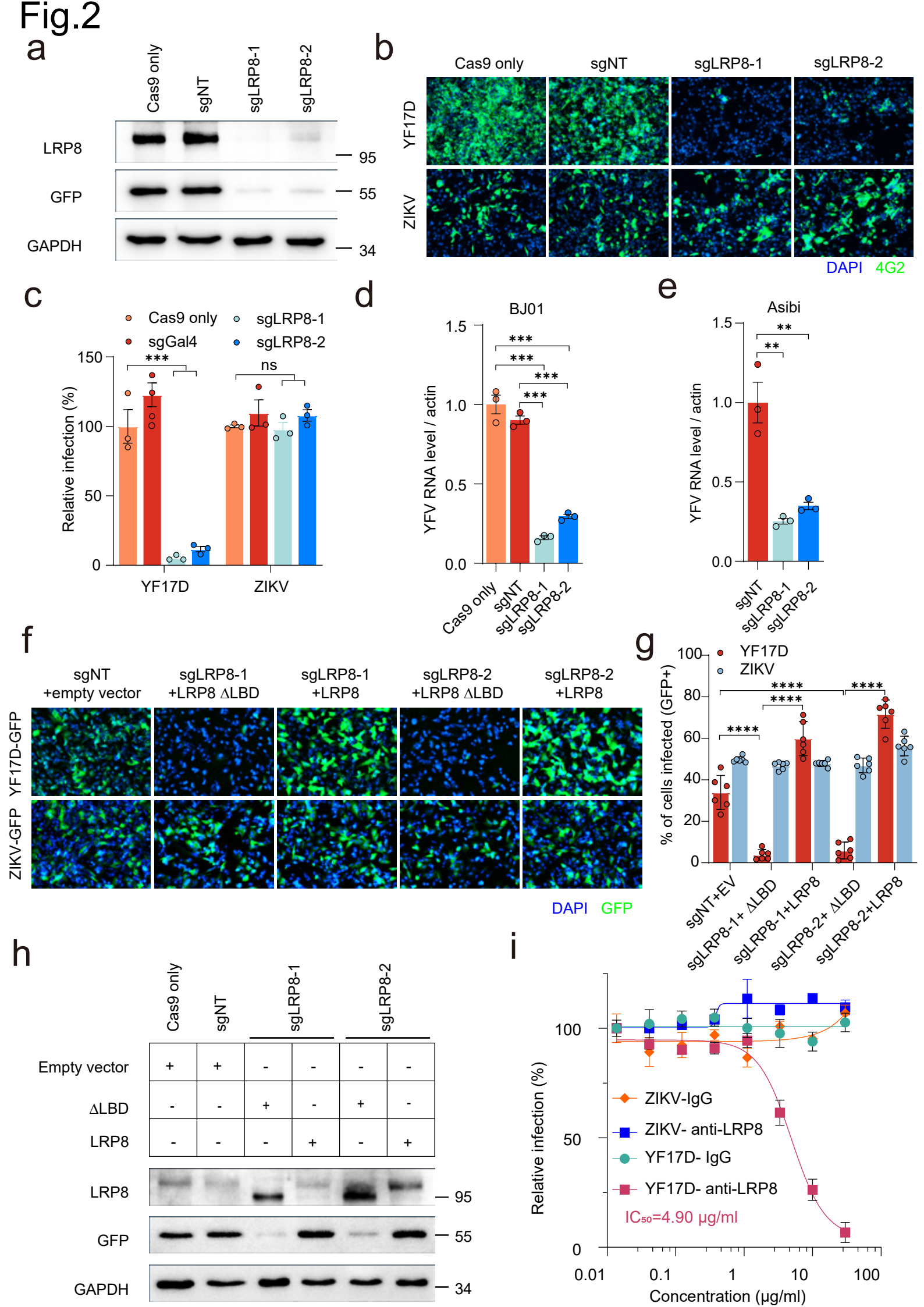
a
Cas9 only
sgNT
sgLRP8-1
sgLRP8-2
LRP8
GFP
GAPDH
95
55
34
b
Cas9 only
sgNT
sgLRP8-1
sgLRP8-2
YF17D
ZIKV
DAPI 4G2
c
Cas9 only
sgGal4
sgLRP8-1
sgLRP8-2
Relative infection (%)
150
100
50
0
***
ns
YF17D
ZIKV
d
BJ01
YFV RNA level / actin
1.5
1.0
0.5
0.0
***
***
***
***
Cas9 only
sgNT
sgLRP8-1
sgLRP8-2
e
Asibi
YFV RNA level / actin
1.5
1.0
0.5
0.0
**
**
sgNT
sgLRP8-1
sgLRP8-2
f
sgNT +empty vector
sgLRP8-1 +LRP8 ΔLBD
sgLRP8-1 +LRP8
sgLRP8-2 +LRP8 ΔLBD
sgLRP8-2 +LRP8
YF17D-GFP
ZIKV-GFP
DAPI GFP
g
YF17D
ZIKV
% of cells infected (GFP+)
100
80
60
40
20
0
****
****
****
****
sgNT+EV
sgLRP8-1+ ΔLBD
sgLRP8-1+LRP8
sgLRP8-2+ ΔLBD
sgLRP8-2+LRP8
h
Cas9 only
sgNT
sgLRP8-1
sgLRP8-2
Empty vector
ΔLBD
LRP8
LRP8
GFP
GAPDH
95
55
34
i
Relative infection (%)
100
50
0
ZIKV-IgG
ZIKV- anti-LRP8
YF17D- IgG
YF17D- anti-LRP8
IC50=4.90 μg/ml
0.01
0.1
1
10
100
Concentration (μg/ml)

Fig.3

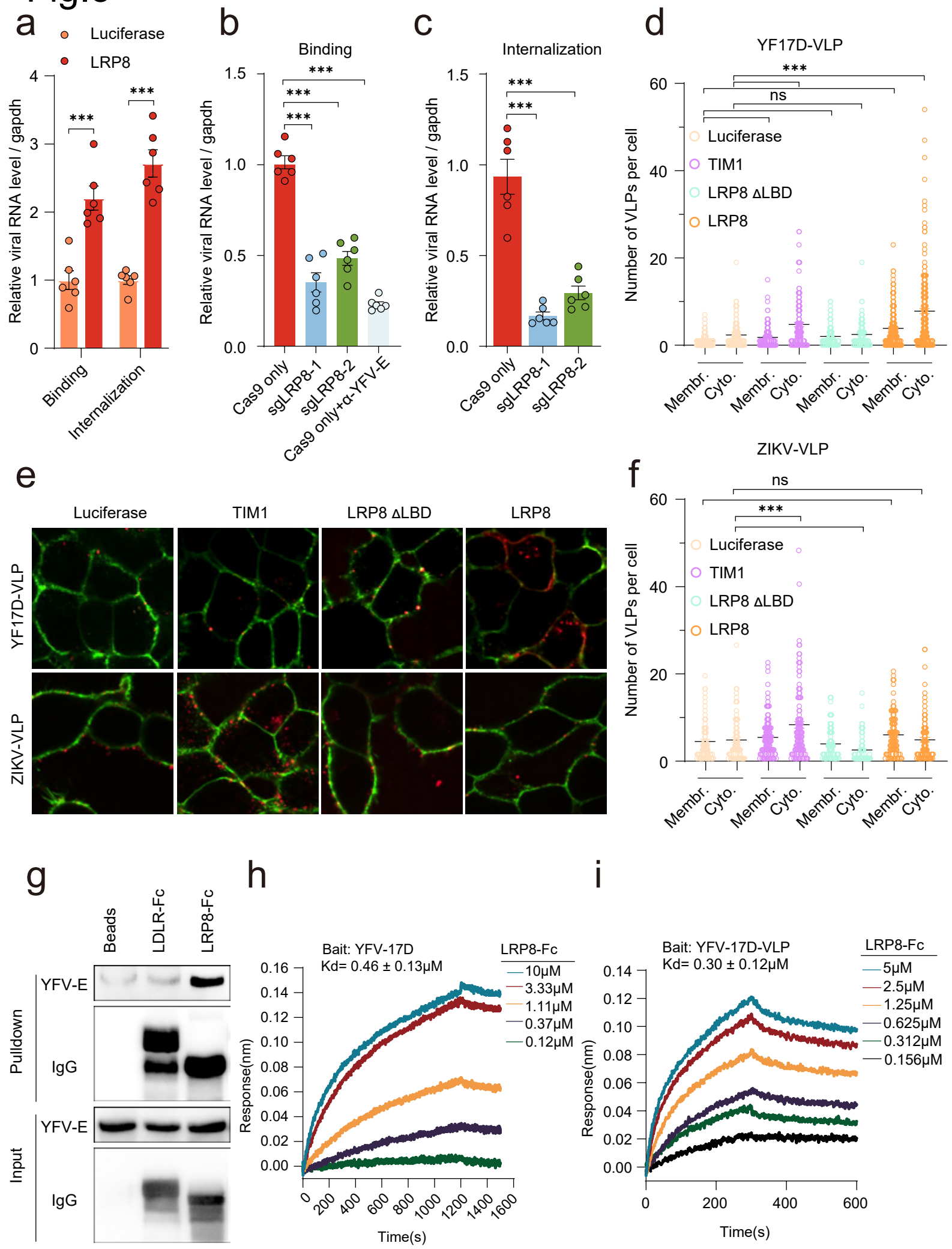
a
Luciferase
LRP8
Relative viral RNA level / gapdh
***
***
Binding
Internalization
b
Binding
Relative viral RNA level / gapdh
***
***
***
Cas9 only
sgLRP8-1
sgLRP8-2
Cas9 only+α-YFV-E
c
Internalization
Relative viral RNA level / gapdh
***
***
Cas9 only
sgLRP8-1
sgLRP8-2
d
YF17D-VLP
Number of VLPs per cell
***
ns
Luciferase
TIM1
LRP8 ΔLBD
LRP8
Membr.
Cyto.
e
Luciferase
TIM1
LRP8 ΔLBD
LRP8
YF17D-VLP
ZIKV-VLP
f
ZIKV-VLP
Number of VLPs per cell
ns
***
Luciferase
TIM1
LRP8 ΔLBD
LRP8
Membr.
Cyto.
g
Beads
LDLR-Fc
LRP8-Fc
Pulldown
YFV-E
IgG
Input
YFV-E
IgG
h
Bait: YFV-17D
Kd= 0.46 ± 0.13μM
LRP8-Fc
10μM
3.33μM
1.11μM
0.37μM
0.12μM
Response(nm)
Time(s)
i
Bait: YFV-17D-VLP
Kd= 0.30 ± 0.12μM
LRP8-Fc
5μM
2.5μM
1.25μM
0.625μM
0.312μM
0.156μM
Response(nm)
Time(s)

Fig.4

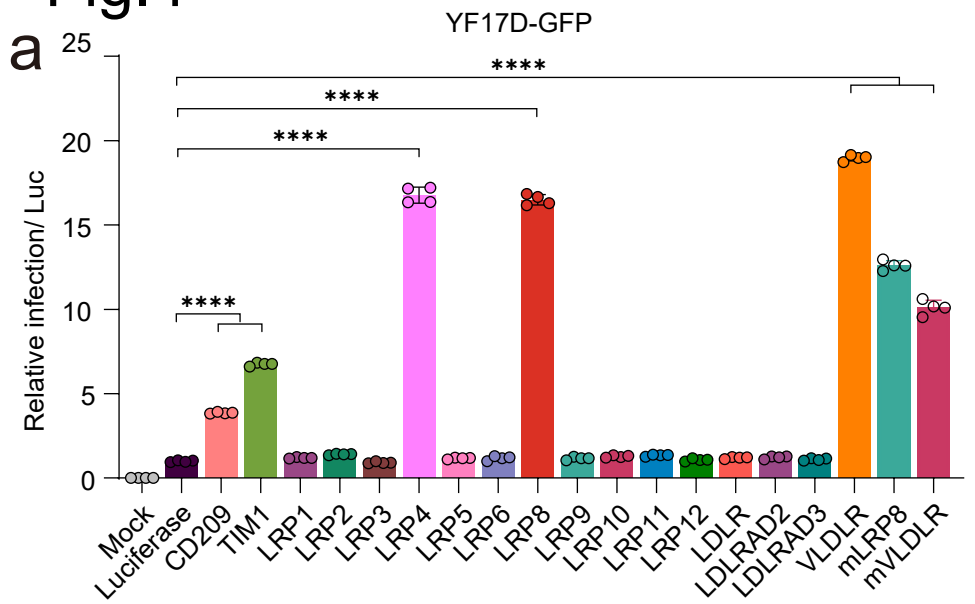
a
YF17D-GFP
Relative infection/ Luc
0
5
10
15
20
25
****
****
****
****
Mock
Luciferase
CD209
TIM1
LRP1
LRP2
LRP3
LRP4
LRP5
LRP6
LRP8
LRP9
LRP10
LRP11
LRP12
LDLR
LDLRAD2
LDLRAD3
VLDLR
mLRP8
mVLDLR

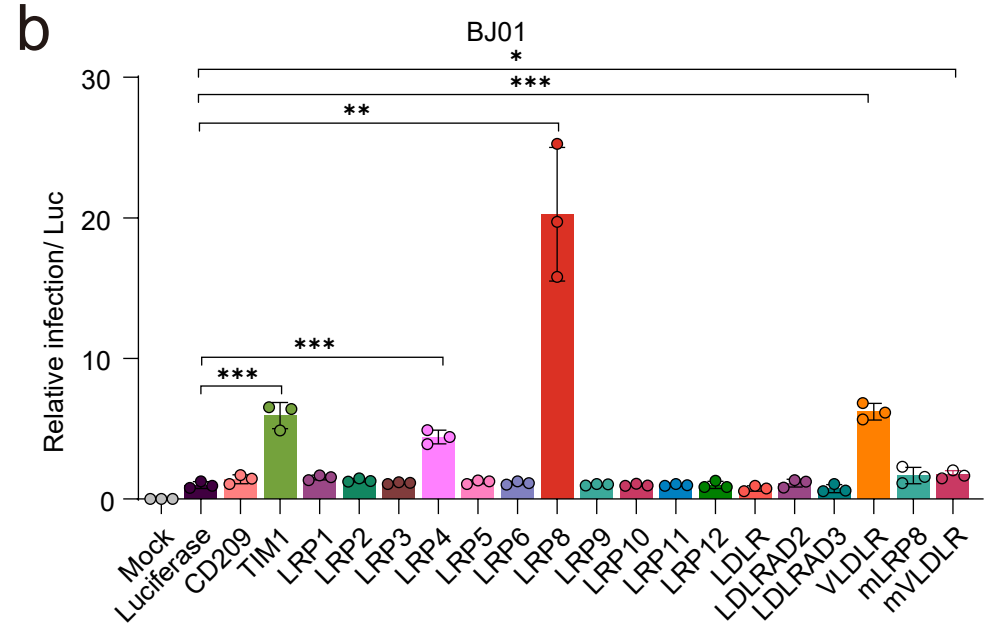
b
BJ01
Relative infection/ Luc
0
10
20
30
*
***
**
***
***
Mock
Luciferase
CD209
TIM1
LRP1
LRP2
LRP3
LRP4
LRP5
LRP6
LRP8
LRP9
LRP10
LRP11
LRP12
LDLR
LDLRAD2
LDLRAD3
VLDLR
mLRP8
mVLDLR

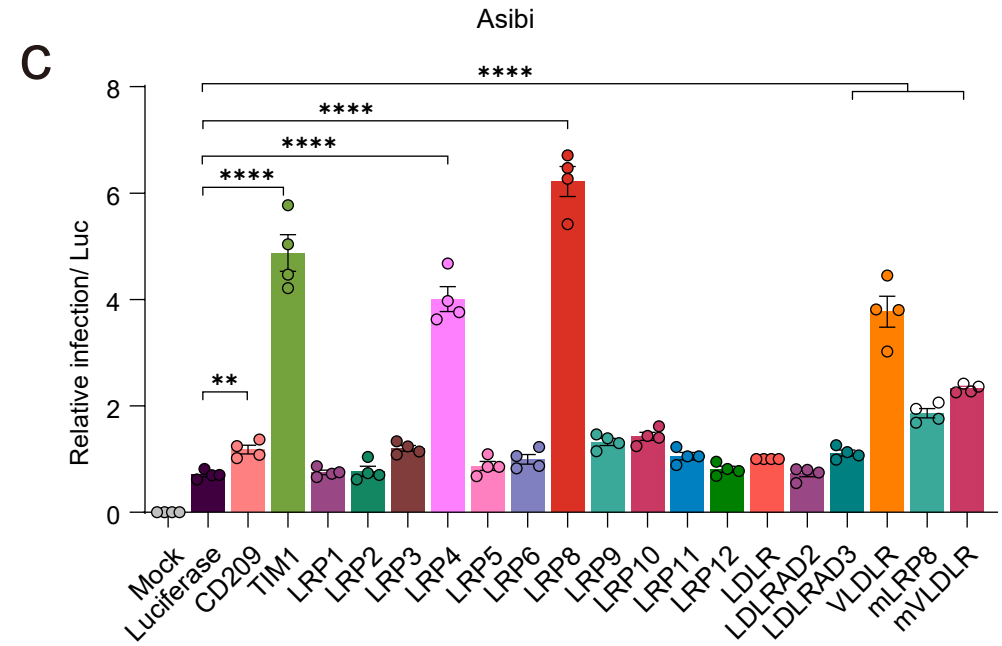
c
Asibi
Relative infection/ Luc
0
2
4
6
8
****
****
****
****
**
Mock
Luciferase
CD209
TIM1
LRP1
LRP2
LRP3
LRP4
LRP5
LRP6
LRP8
LRP9
LRP10
LRP11
LRP12
LDLR
LDLRAD2
LDLRAD3
VLDLR
mLRP8
mVLDLR

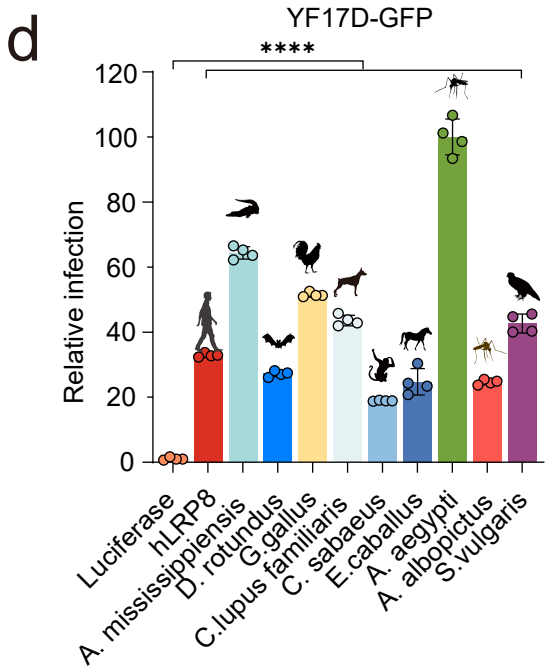
d
YF17D-GFP
Relative infection
0
20
40
60
80
100
120
****
Luciferase
hLRP8
A. mississippiensis
D. rotundus
G.gallus
C.lupus familiaris
C. sabaeus
E.caballus
A. aegypti
A. albopictus
S.vulgaris

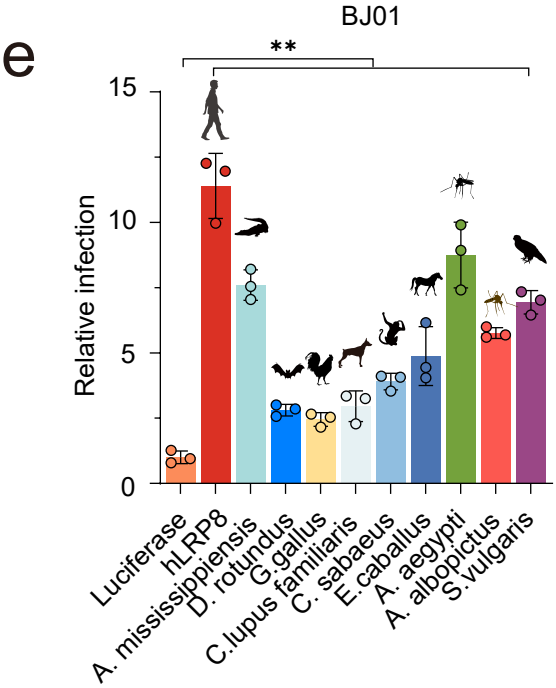
e
BJ01
Relative infection
0
5
10
15
**
Luciferase
hLRP8
A. mississippiensis
D. rotundus
G.gallus
C.lupus familiaris
C. sabaeus
E.caballus
A. aegypti
A. albopictus
S.vulgaris

Fig.5

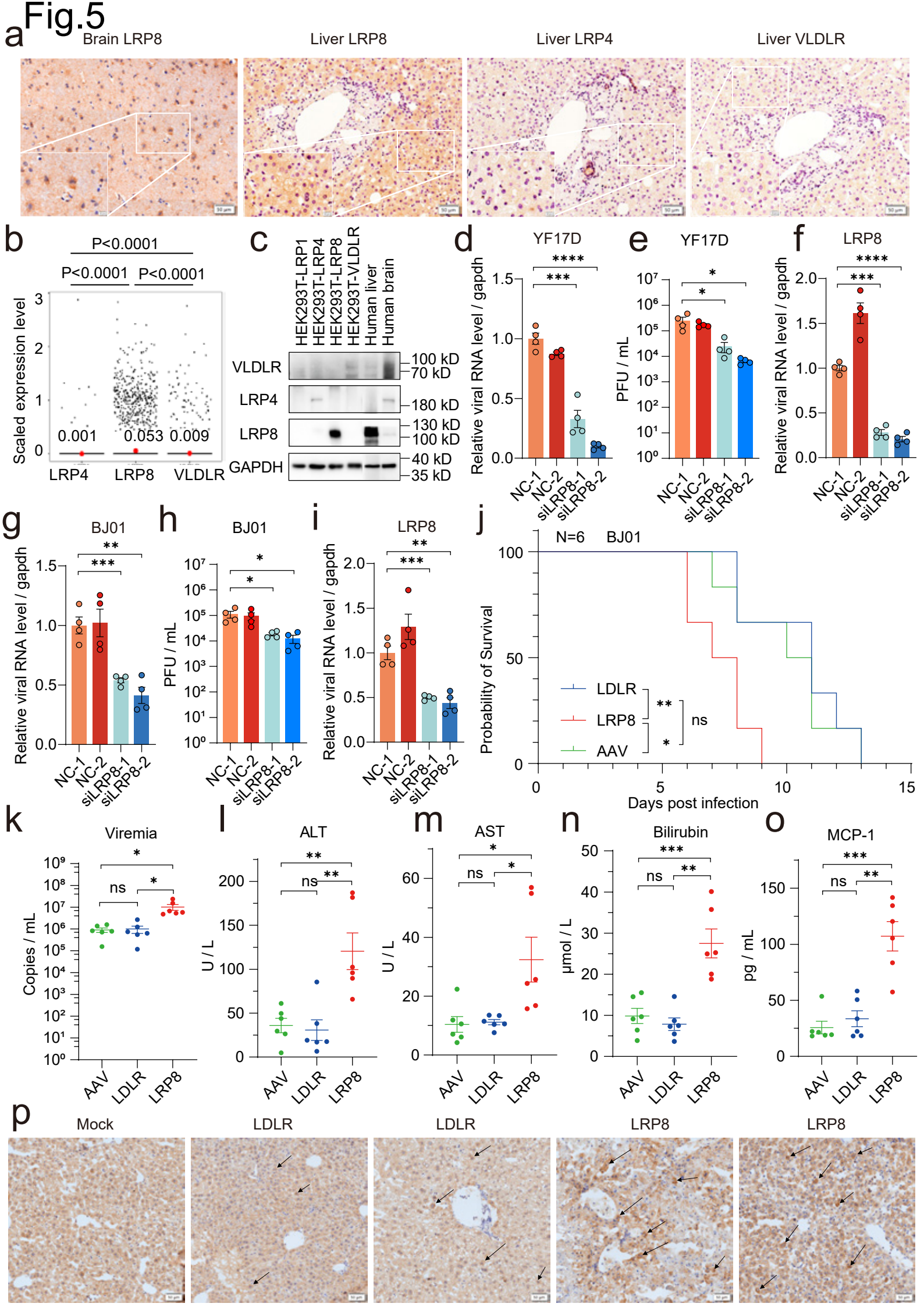
a
Brain LRP8
Liver LRP8
Liver LRP4
Liver VLDLR
b
P<0.0001
P<0.0001
P<0.0001
Scaled expression level
0.001
0.053
0.009
LRP4
LRP8
VLDLR
c
HEK293T-LRP1
HEK293T-LRP4
HEK293T-LRP8
HEK293T-VLDLR
Human liver
Human brain
VLDLR
LRP4
LRP8
GAPDH
100 kD
70 kD
180 kD
130 kD
100 kD
40 kD
35 kD
d
YF17D
Relative viral RNA level / gapdh
NC-1
NC-2
siLRP8-1
siLRP8-2
e
YF17D
PFU / mL
f
LRP8
Relative viral RNA level / gapdh
g
BJ01
Relative viral RNA level / gapdh
h
BJ01
PFU / mL
i
LRP8
Relative viral RNA level / gapdh
j
N=6 BJ01
Probability of Survival
Days post infection
LDLR
LRP8
AAV
ns
k
Viremia
Copies / mL
AAV
LDLR
LRP8
l
ALT
U / L
m
AST
U / L
n
Bilirubin
μmol / L
o
MCP-1
pg / mL
p
Mock
LDLR
LDLR
LRP8
LRP8

Fig.6

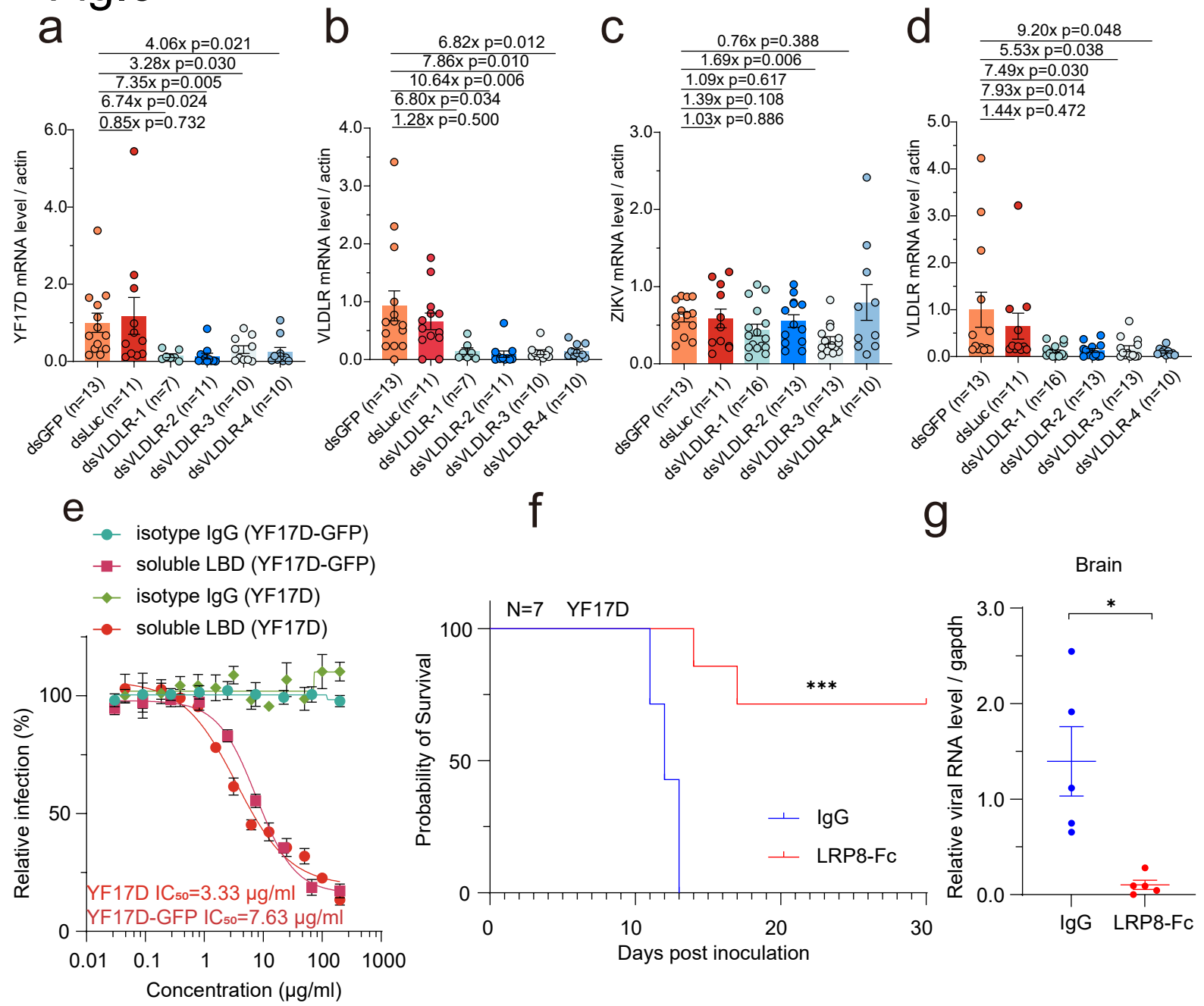
a
4.06x p=0.021
3.28x p=0.030
7.35x p=0.005
6.74x p=0.024
0.85x p=0.732
YF17D mRNA level / actin
dsGFP (n=13)
dsLuc (n=11)
dsVLDLR-1 (n=7)
dsVLDLR-2 (n=11)
dsVLDLR-3 (n=10)
dsVLDLR-4 (n=10)
b
6.82x p=0.012
7.86x p=0.010
10.64x p=0.006
6.80x p=0.034
1.28x p=0.500
VLDLR mRNA level / actin
c
0.76x p=0.388
1.69x p=0.006
1.09x p=0.617
1.39x p=0.108
1.03x p=0.886
ZIKV mRNA level / actin
dsVLDLR-1 (n=16)
dsVLDLR-2 (n=13)
dsVLDLR-3 (n=13)
d
9.20x p=0.048
5.53x p=0.038
7.49x p=0.030
7.93x p=0.014
1.44x p=0.472
e
isotype IgG (YF17D-GFP)
soluble LBD (YF17D-GFP)
isotype IgG (YF17D)
soluble LBD (YF17D)
Relative infection (%)
YF17D IC50=3.33 μg/ml
YF17D-GFP IC50=7.63 μg/ml
Concentration (μg/ml)
f
N=7 YF17D
Probability of Survival
***
IgG
LRP8-Fc
Days post inoculation
g
Brain
Relative viral RNA level / gapdh
*
IgG
LRP8-Fc

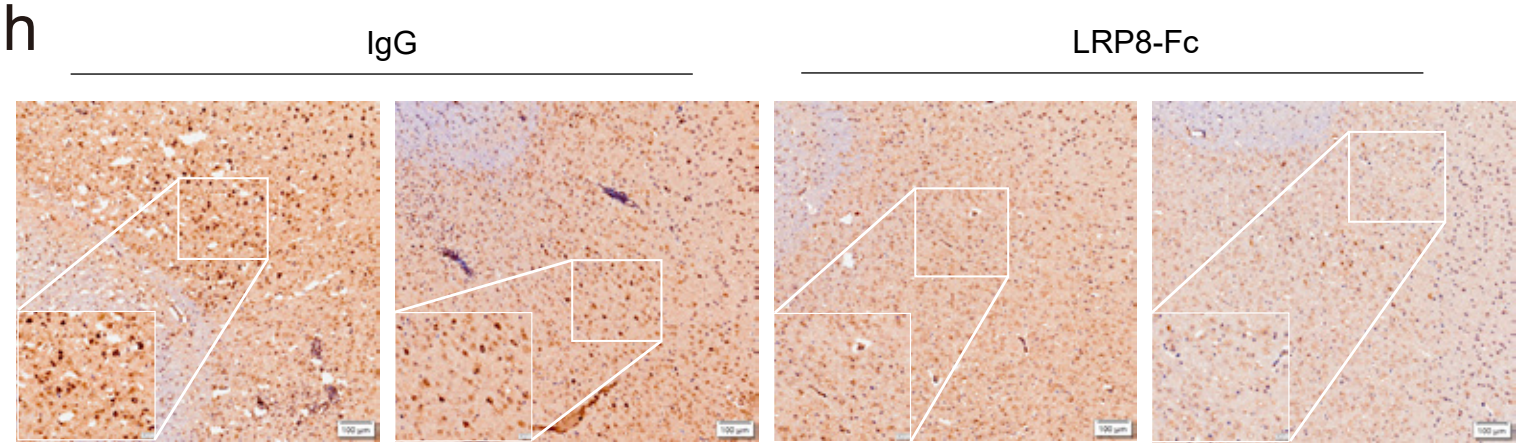
h
IgG
LRP8-Fc

Extended Figures

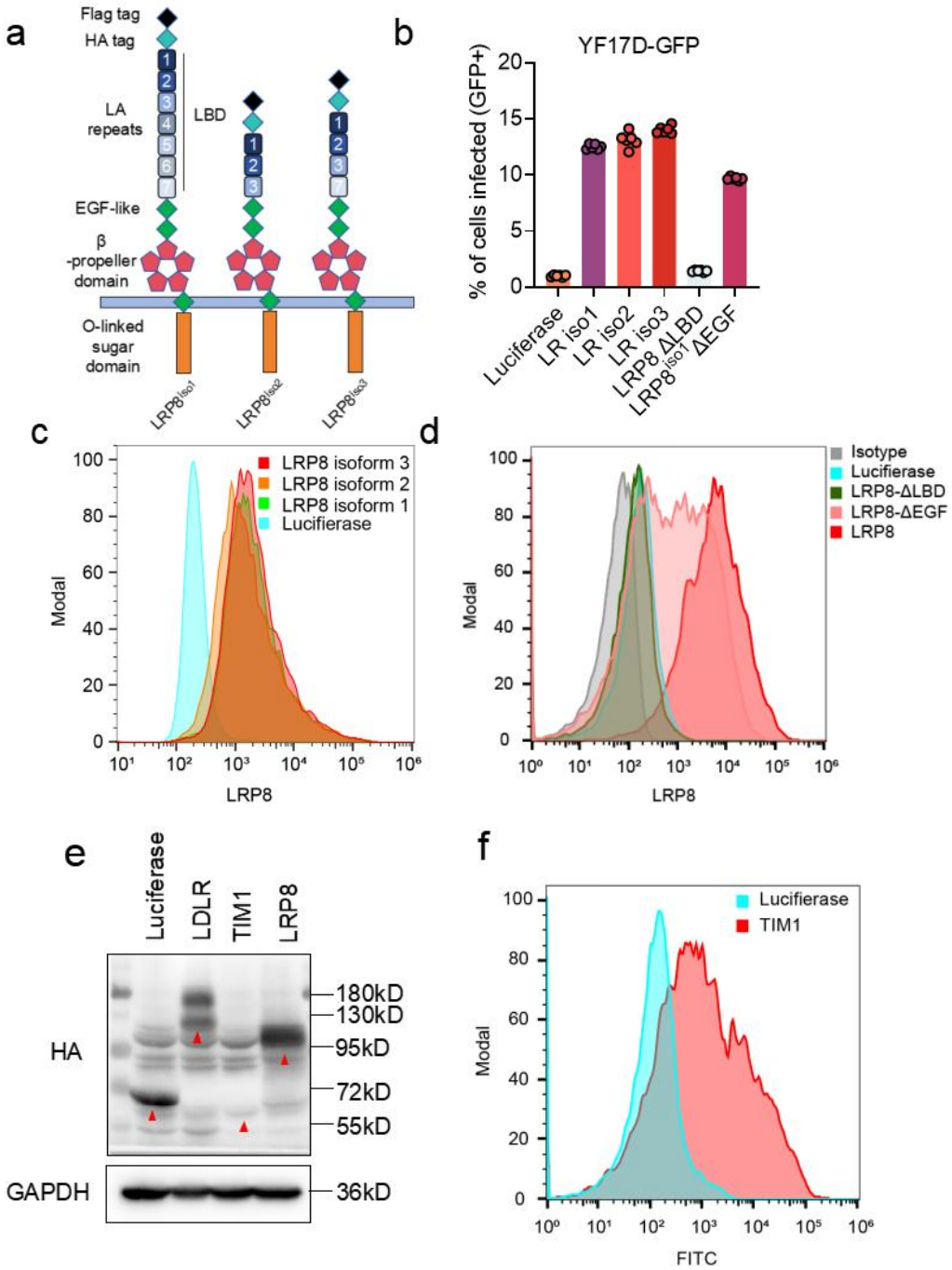

Extended Figure 1 Different major isoforms of LRP8 have similar activities in promoting YF infection. a, Schematic structure of LRP8 isoforms; **b,** In HEK293T cells, luciferase, LRP8 isoforms and its truncations were transiently overexpressed and the cells are infected by YFV 17D pseudoviruses. The ratios of infected cells were analyzed using FACS at 24hpi. **c,d,** Expression of the isoforms and its truncations on cell surface were determined with anti-LRP8 by FACS. **e, f**, Luciferase, LDLR, LRP8 or TIM1 containing 3xHA tag were analyzed by western blot in HEK293T cells or FACS.

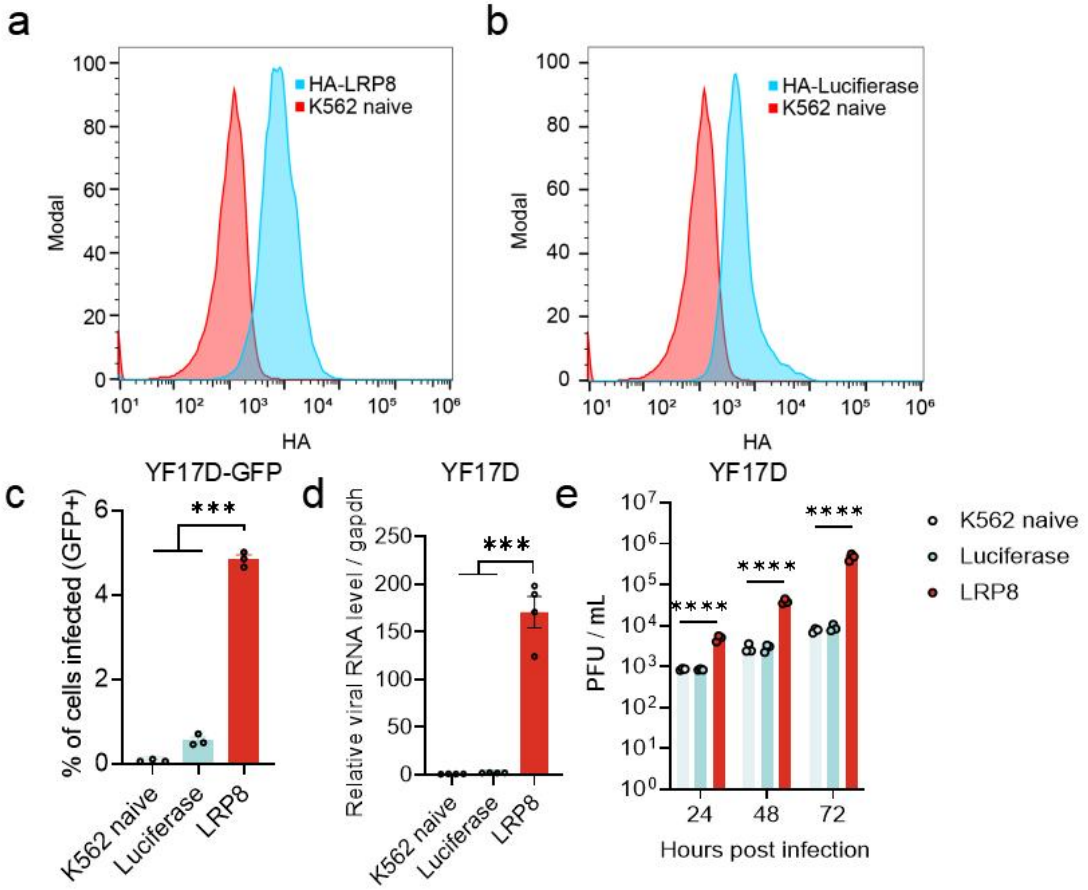

Extended Figure 2 LRP8 promotes YF17D infection in K562 cells. a, b. LRP8 and luciferase expression on K562 cell surface were determined by FACS with HA antibody staining. **c**. In K562 cells, HA-tagged luciferase and LRP8 were stably overexpressed and the cells are infected by YFV 17D pseudoviruses and the infection rates were determined by FACS at 24 hpi. **d**. In K562 cells, HA-tagged luciferase and LRP8 were stably overexpressed and the cells are infected by live YFV 17D and viral RNA level in cells were determined by qRT-PCR at 48 hpi. **e**. Infectious viral particles from d were determined by plaque assay.

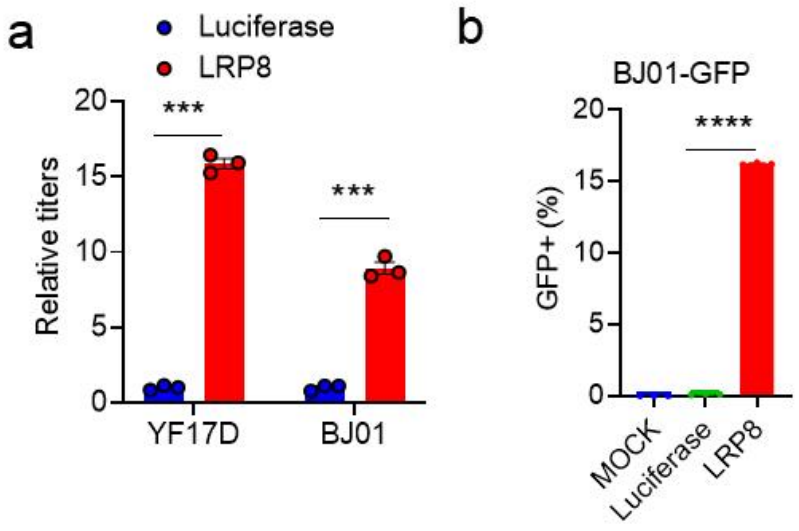

Extended Figure 3 LRP8 promotes the infection by live viruses of YF17D, BJ01 and BJ01-GFP pseudovirus. a. Supernatant of HEK293T expressing Luciferase and LRP8 infected with YF17D (0.05 MOI) and BJ01(0.05 MOI). At 48hpi, the viral titers were determined by plaque assay in BHK21 cells. **b**. In HEK293T cells, luciferase and LRP8 were transiently overexpressed and the cells are infected by YFV BJ01 pseudoviruses. The ratios of infected cells were analyzed using FACS at 24 hpi.

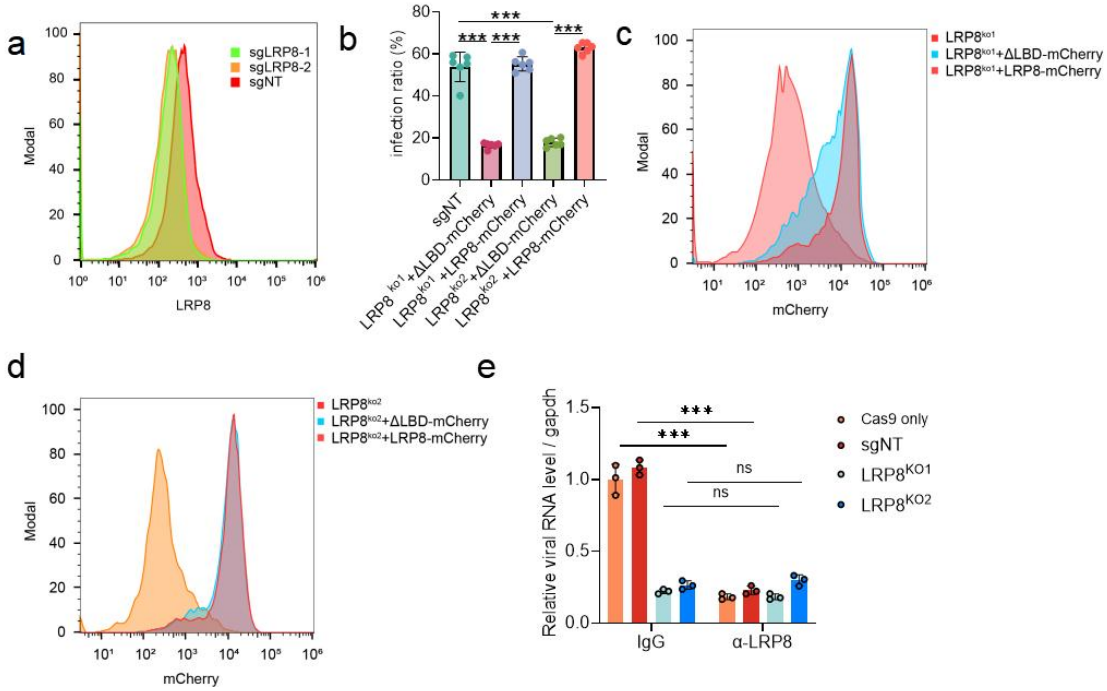

Extended Figure 4 Deficiency of LRP8 decreases live YF17D infection. a. U87MG cells expressing Cas9/sgLRP8 single clones and Cas9 only were tested by FACS with anti-LRP8. **b-d**, In two wells LRP8 KO cells, ΔLBD-mCherry and LRP8-mcherry plasmids were electroporated. 48h later the cells are infected with YF17D. 48 hpi the cells were stained for E protein and quantitated by fluorescence microscope. ΔLBD-mCherry and LRP8-mcherry expressions were determined by FACS. **e**. U87MG-sgLRP8 and control U87MG cells expressing only Cas9 were preincubated with 10 μg/ml anti-LRP8 (sc-1A1) or IgG before being infected by YF17D. 48 hpi, the infections were analyzed by qRT-PCR.

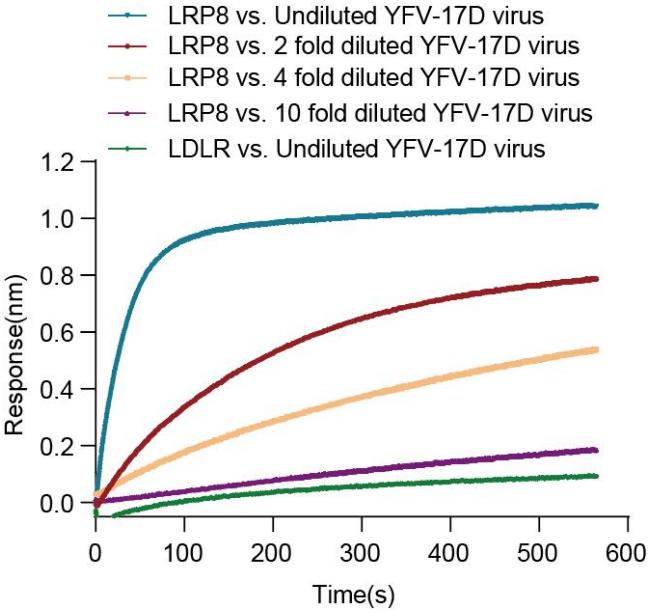

Extended Figure 5 Purified LRP8 LBD or LDLR LBD were biotinated and immobilized on the probe of biolayer inferometry (BLI). The binding of YFV 17D viral particles to LRP8 or LDLR was measured by BLI assay.

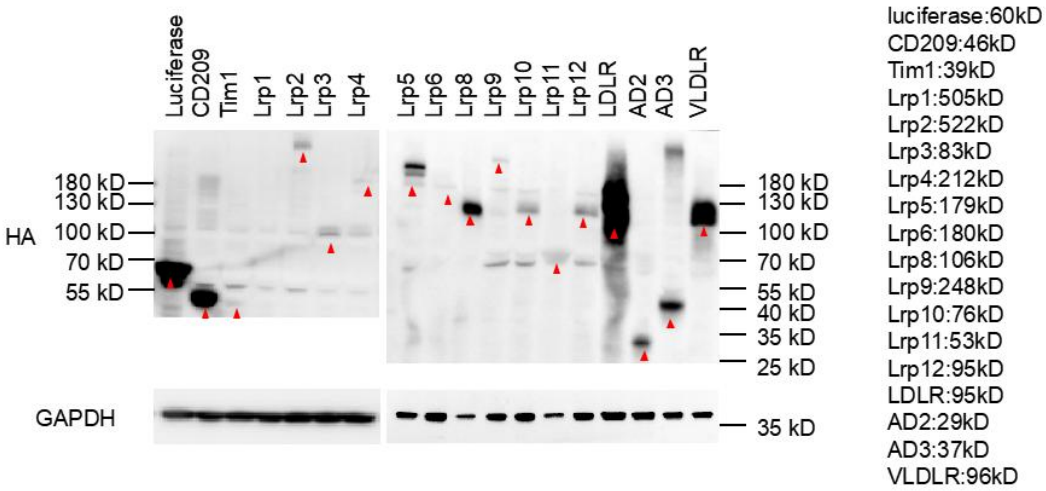

Extended Figure 6 Expression of different members of the LDLR family. In HEK293T cells, plasmids expressing different LDLR family members were transfected into HEK293T for 48 hours and the target protein containing 3X HA tag were analyzed by Western blot. The corresponding molecular weight of each protein were marked at the right of figure.

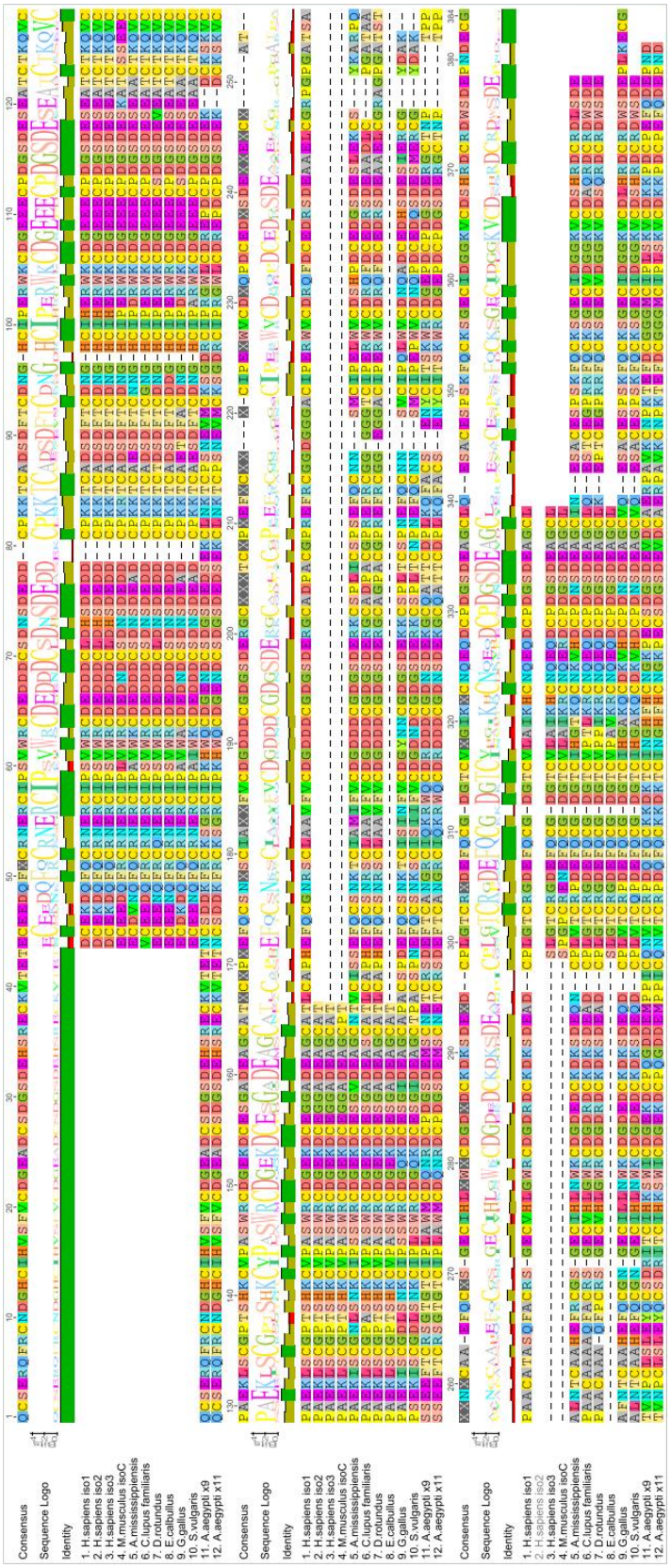

Extended Figure 7 The amino acid sequence alignment of LRP8 ligand binding domain (LBD). The LRP8 LBD amino acid sequences of human, mouse, mosquito, A. mississippiensis, bat, chicken, bird, dog, horse, green monkey were downloaded from NCBI and aligned using Geneious software.

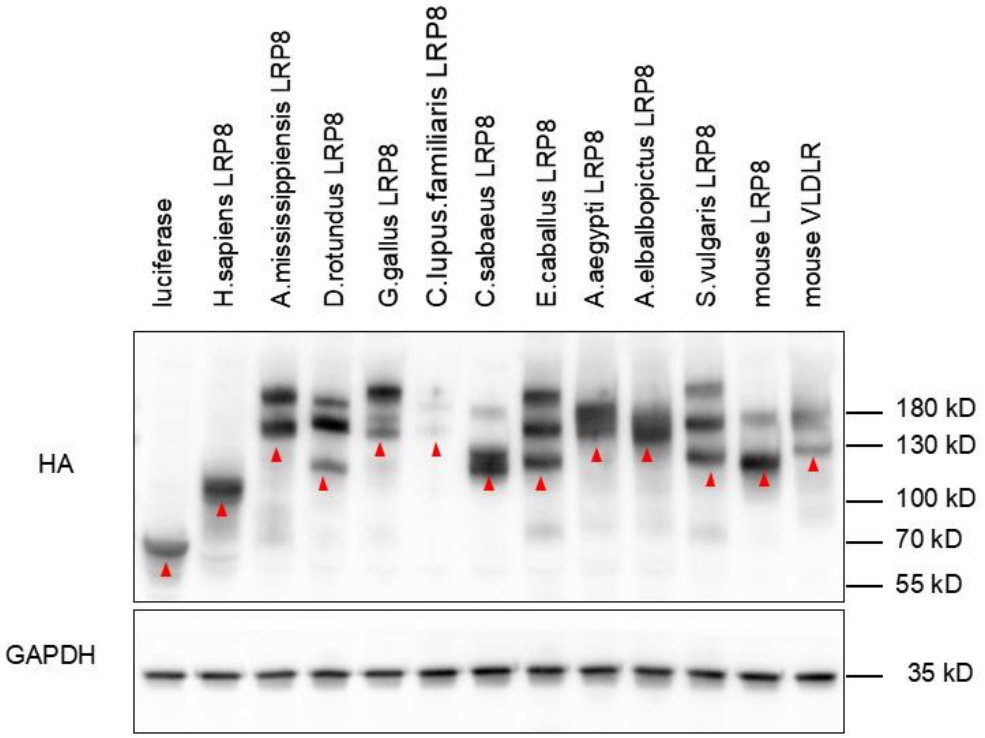

Extended Figure 8 Expression of LRP8 homologs from different species. In HEK293T cells, plasmids expressing different LRP8 orthologs were transfected into HEK293T for 48 hours and the target protein containing 3X HA tag were analyzed by Western blot.

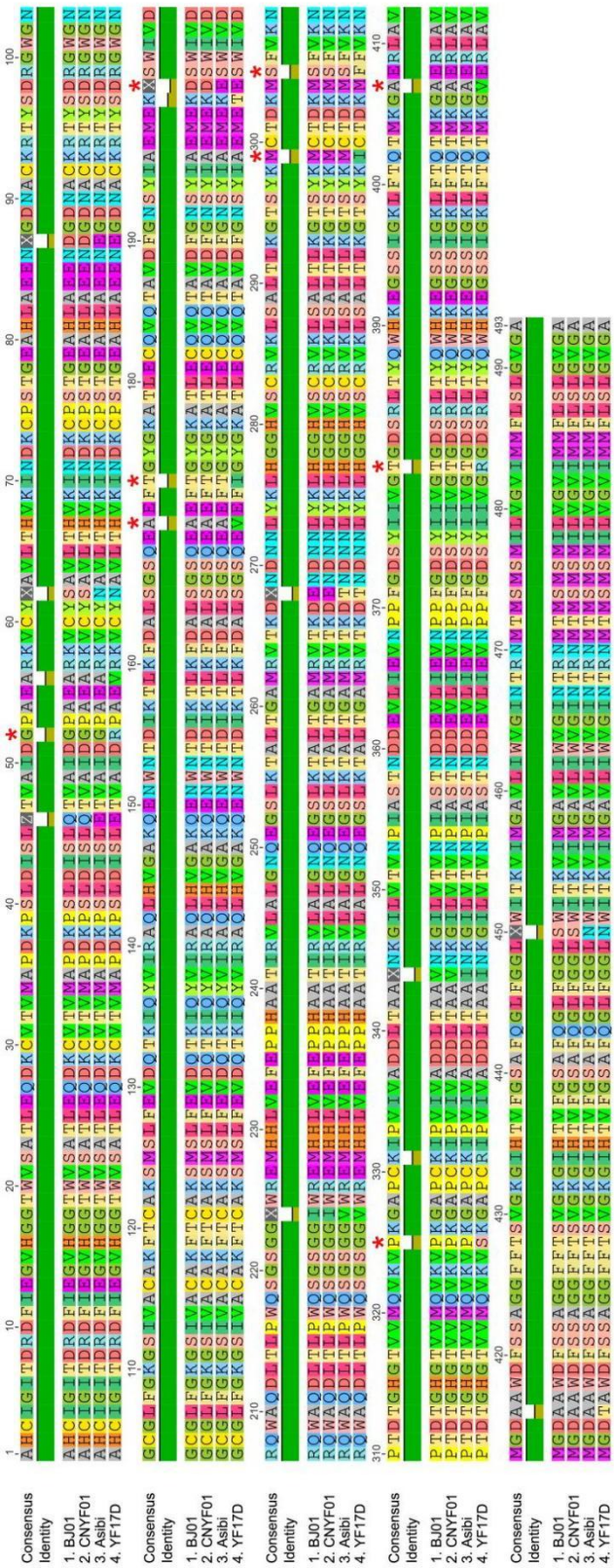

Extended Figure 9 The amino acid sequence alignment of YF strain envelope proteins. The amino acid sequence of the envelope protein of YF BJ01, CNYF01, Asibi, YF17D strains were downloaded from NCBI and aligned using Geneious software. Asterisks indicate sites of mutations in E.

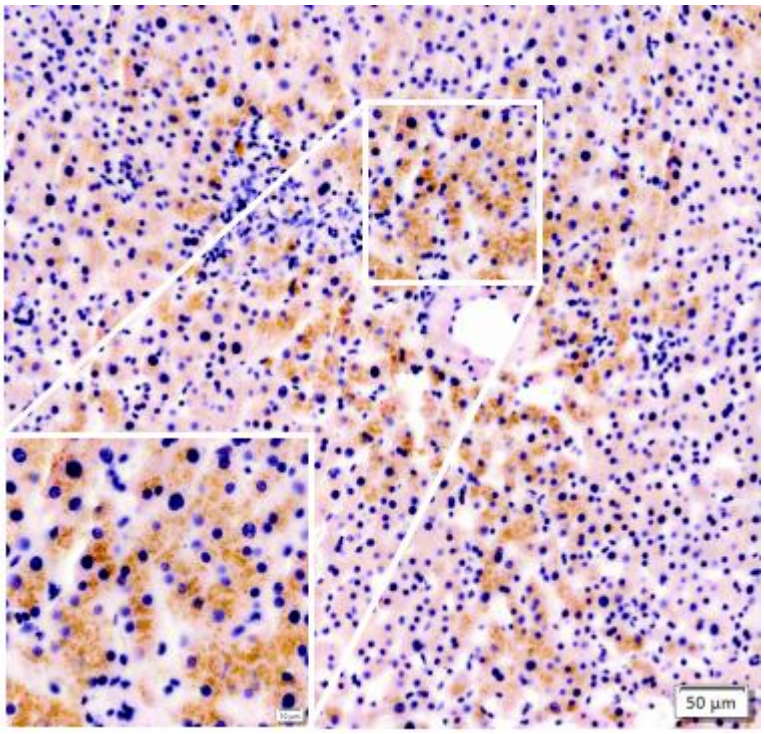

Extended Figure 10 LRP8 expression were determined in human liver sample by immunohistochemistry staining with a LRP8 antibody (Thermo 3H2 clone).

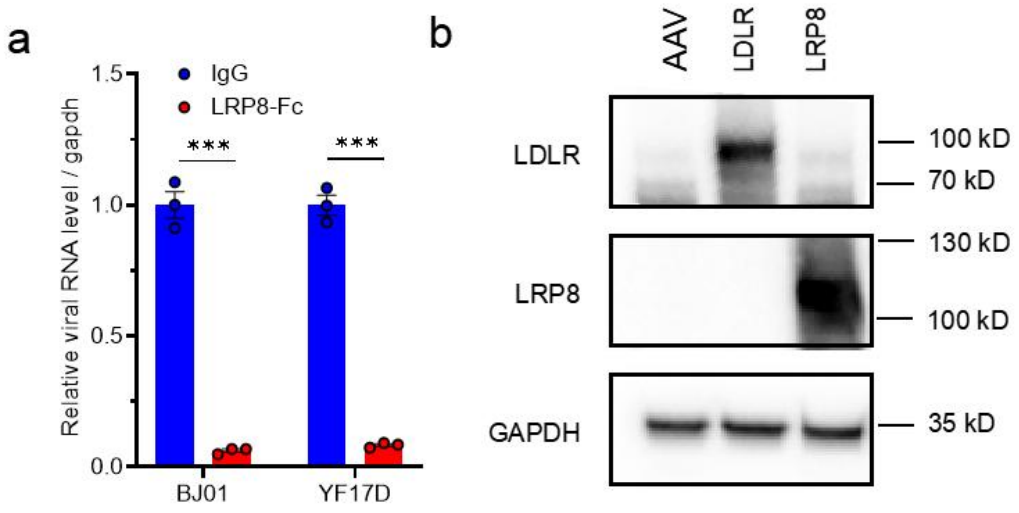

Extended Figure 11 Soluble LRP8-Fc blocks BJ01 and YF17D infection and validation of the expression of LDLR and LRP8 delivered by AAV in mouse liver. a. Preincubation of soluble LRP8 (200 μg/ml) with 0.5 MOI of BJ01 and Asibi for 1 hour, and the protein-virus mixture were added into PHHs for 48 hours. The viral RNA was quantified by qRT-PCR (three biological repeats). **b**. hLDLR and hLRP8 in mouse liver were determined at 3 weeks post AAV delivering by Western blot.

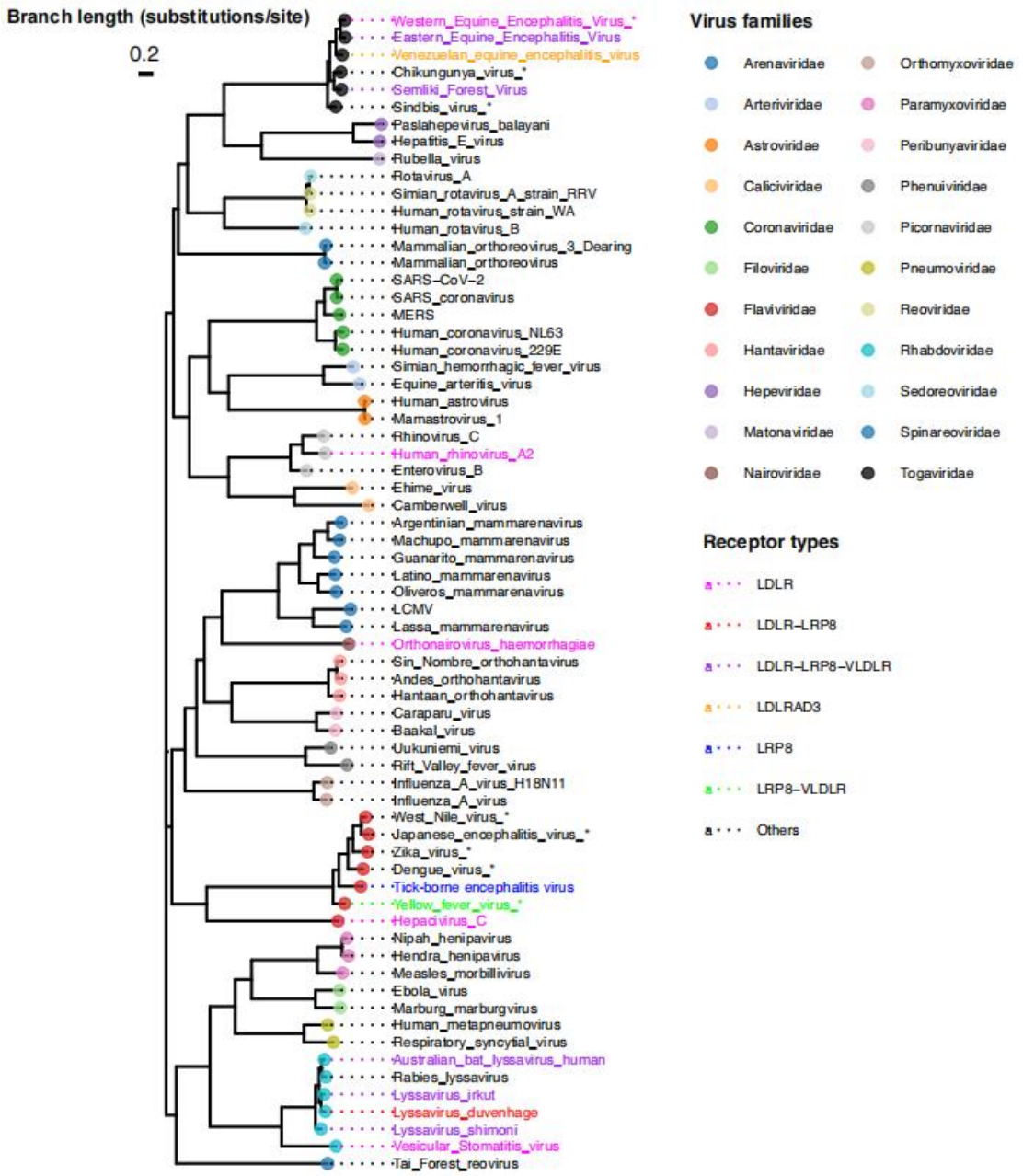

Extended Figure 12 Phylogenetic Tree Construction of RNA Virus RdRPs. To investigate the evolutionary relationships of RNA-dependent RNA polymerases (RdRPs) among human-infecting RNA viruses, we curated 24 RNA virus families from the Virus-Host Database. Receptor-annotated viruses were identified via the ViralReceptor database, covering 17 families. RdRP protein sequences were collected from NCBI, GenBank, and UniProtKB/Swiss-Prot. Among 94 viruses, all except Hepatitis delta virus, Echovirus E8, and Retroviridae had identifiable RdRPs, yielding 22 families for analysis. Sequences were aligned using MAFFT (v7.526) with the --localpair --maxiterate 1000 options, and a maximum likelihood tree was built with FastTree (v2.1.11). Visualization was done using ggtree (v3.21) in R (v4.4.3), highlighting families with known human receptors. Asterisks indicate mosquito-borne viruses.